Cranfield UNIVERSITY

Effect of Surface Suction on Cross-Flow Instability and Transition Occuring Near a Swept Attachment-Line

A. Smith
D.I.A. Poll

COA report No. 9802
1998

Flow Control and Prediction
College of Aeronautics
Cranfield University
Cranfield
Bedford MK43 0AL
England

College of Aeronautics Report No. 9802
1998

ISBN 1 871564 999

"The views expressed herein are those of the author/s alone and do not necessarily represent those of the University"

Flow control and Prediction
College of Aeronautics
Cranfield University
Cranfield
Bedford MK43 0AL
England

Contents

Acknowledgements

This work was funded by the DTI through DERA (Bedford) on contract number ASF 2622U. Thanks go to Dr Ashill and Mrs Betts for their support and advice throughout the work.

Notation

η	viscous length scale (m)
ν	kinematic viscosity (m^2 /s)
ρ	density (kg/m^3)
C	chord (m)
C_q	suction coefficient
d_h	hole diameter (m)
D	model diameter (m)
f	frequency (Hz)
p_a	attachment line static pressure (N/m^2)
p_s	static pressure (N/m^2)
q	dynamic pressure (N/m^2)
Q	freestream velocity (m/s)
$\overline{Q}$	empty tunnel freestream velocity (m/s)
$\overline{R}$	leading edge Reynolds number
$R_{\theta lam}$	attachment-line transition Reynolds number based on laminar momentum thickness
s	general spanwise distance (m)
s_{TT}	spanwise distance from the start of the suction surface (mm)
U	chordwise velocity (m/s)
V	spanwise velocity (m/s)
x	chordwise distance (m)

Subscripts

∞	freestream conditions

1 Introduction

Advances in aviation during and following the Second World War led to an enormous improvement in the performance of aircraft. The push for enhanced efficiency brought cruise speeds into the transonic range, where the associated drag rise due to the appearance of shock-waves became a limiting factor. Wing sweep was adopted to delay the onset of this drag rise, but with this development came several new and unforeseen problems.

Preliminary theoretical work assumed that the boundary layer transition characteristics on a swept wing would be subject to the independence principle, so the chordwise transition position could be predicted from two-dimensional data. However, during flight tests on swept wing aircraft by Gray in 1952[1,2], transition due to cross-flow instability, with its characteristic 'saw-tooth' transition front, was discovered. Attachment-line contamination was also observed, but was not identified as an independent transition mechanism. Gray concluded that, as sweep angles increased beyond 20°, the transition front moved swiftly towards the leading edge and, at larger sweep angles, transition occurred at the leading edge itself. Subsequently, cross flow instability was demonstrated theoretically by Owen and Randall[3,4] and Stuart[5], and confirmed experimentally by Anscombe and Illingworth[6] and Gregory and Walker[5]. Ten years later, laminar flow projects were launched by Northrop and Handley Page, both incorporating wing sections designed to avoid cross-flow instability by the application of suction through a series of narrow slots. However, during initial flight tests, it was found that transition occurred close to the leading edge and very little laminar flow was obtained. Working independently, both groups identified the mechanism as contamination of the wing attachment-line by the turbulent fuselage boundary layer, via the wing-body junction. The turbulent attachment-line then contaminated the flow over the whole chord and laminar flow, if any, was only obtained near the wing tips. Consequently, investigations were started in the early 1960's, by Pfenninger at Northrop, Gregory at the National Physical Laboratory, and Gaster at the College of Aeronautics, Cranfield, to investigate this 'new' transition mechanism. Attachment-line transition was quickly identified as an independent mechanism and several ideas were proposed for its control[7,8]. However, by that time, commercial interest in laminar flow had waned and funding for the research was stopped. However, following the oil crisis of the early 1970's interest in laminar leading edge flows resumed with a number of initiatives, especially the NASA Aircraft Energy Efficiency/Laminar Flow Control (ACEE/LFC) research programs and, in 1975, the Eurovisc Working Party on Transition in Boundary Layers made swept wing research its primary focus. Since then there has been a continuous, world-wide, effort on the problem- including a German national research programme on transonic wing technology set up in 1985. NASA has sponsored a substantial flight-test program, including a Lockheed Jetstar[9] and a Boeing 757 in simulated airline service[10].

Gas turbine development has now reached a point where additional increases in efficiency are both difficult and expensive to achieve. Consequently, aircraft manufacturers are looking elsewhere for ways to reduce Direct Operating Costs (DOC) or to increase performance. The attention of industry is currently focusing on hybrid laminar flow control (HLFC) as a possible method of reducing DOC for civil aircraft.

The combination of a natural laminar flow aerofoil and active flow control at the leading edge can produce laminar flow over 50-60% of the upper surface of a wing, leading to a reduction in total drag of up to 15%[11]. By further extending the use of laminar flow control to tail fins, engine nacelles and pylons the potential reduction in drag becomes very significant.

The work contained in this report is concerned with the use of transpiration at the leading edge of swept wings to modify and control transition due to cross-flow instability. Transition conditions are identified on both porous and non-porous surfaces, with and without suction, and the effect of two-dimensional excrescences is considered. Throughout, the application of the results to vehicle design is stressed and, where possible, simple design criteria are presented.

2 The Swept Wing Boundary Layer

2.1 General Swept Conditions

As an aircraft's speed increases the freestream Mach number increases and eventually, at some particular point on the wing surface, the local flow speed reaches sonic conditions. At still higher speeds, a small region of supersonic flow is established which is terminated by a shock wave. The interaction of this shock wave with the wing boundary layer causes an increase in drag and may produce shock-stall if the adverse pressure gradient associated with the shock wave causes the boundary layer to separate. The onset of this drag rise can be delayed to higher flight speeds by sweeping the wing and this is the technique currently employed.

2.2 The Attachment-Line and Infinite Swept Conditions

An important consequence of wing sweep is the creation of an attachment-line flow. Referring to Figure 1, the freestream can be resolved into two components; the chordwise flow and a spanwise flow. The attachment line is defined as the line along the leading edge, which separates the flow passing over the upper surface from that passing over the lower surface. The streamline pattern around a swept leading edge is shown in the figure, with the attachment-line indicated by the line A-A. It can be seen that the flow close to the attachment-line is characterised by curved streamlines and, consequently, the boundary layer is highly three-dimensional. The condition of the attachment-line has an important effect on the state of the boundary layer over the rest of the wing, since fluid from the attachment line remains within the wing boundary layer.

To simplify study of the physics of leading edge flow, it is convenient to reduce the number of independent variables by aiming for infinite swept conditions. A model with constant spanwise geometry can be used to produce a boundary layer with spanwise independent properties (e.g. boundary layer thickness, skin friction, the rate of divergence, etc.) provided the boundary layer is either laminar or turbulent, but not transitional[12]. The spanwise independence is achieved by a balance between the transfer of fluid from the attachment-line into the chordwise boundary layer and the entrainment of fluid from the freestream into the attachment-line boundary layer.

2.3 Cross-Flow Instability

All three-dimensional boundary layers are characterised by the presence of streamline curvature. Outside the viscous layer, this curvature is maintained by pressure gradients that act in a direction perpendicular to the external streamline direction, in planes drawn parallel to the surface. As the surface is approached fluid is slowed by

viscosity and moves in the direction of these gradients to create a "cross-flow" velocity component within the boundary layer. For the cross-flow component of the profile, the boundary conditions are no slip at the surface and zero velocity at the edge of the boundary layer. It follows that such a profile contains at least one point of inflection and, consequently, as demonstrated by Gregory *et al*[13], these profiles become unstable at very low characteristic Reynolds numbers.

2.4 Intermittency

When a boundary layer is in the transitional state, the flow parameters at a fixed measuring station are found to switch almost instantaneously between the laminar and turbulent conditions. This characteristic was recognised by Emmons[14] who introduced the concept of the intermittency, Γ. This is the probability that, at a particular time, t, the flow at a given location is turbulent. Therefore, for purely laminar flow the intermittency is zero and for fully turbulent flow the intermittency is unity.

2.5 Receptivity

Receptivity[15,16,17] is the mechanism by which environmental disturbances enter a laminar boundary layer and interact with the flow to produce instability waves. The normal transition process occurs due to the amplification of these instability waves through linear and non-linear phases until a turbulent flow is established. Bypass transition describes a process by which large, finite amplitude disturbances (for example from a large roughness element) amplify non-linearly and cause transition, "bypassing" the linear amplification phase.

2.6 Parameters Used for The Study of Attachment-Line Flows

The flow field at the leading edge of a wing is governed by many parameters and restrictions need to be applied to the experimental system to reduce the problem to manageable proportions. A simple approach is the use of a model with constant spanwise section to give infinite swept conditions. Moreover, the effects of compressibility can be ignored if the spanwise Mach number at the edge of the attachment-line boundary layer is less than 0.2.

With these constraints, steady, incompressible flow without heat transfer, along an infinite-swept, attachment line is completely determined by the magnitude of the characteristic Reynolds number, $\overline{R}$. By analogy with the Blasius flow, the appropriate viscous length scale, η, is,

$$\eta = \left[\frac{\nu}{dU_e / dx} \right]_{x=0}^{\frac{1}{2}}$$

where **U** is the chordwise velocity at the edge of the viscous layer and **x** is the chordwise position, measured along the surface with the origin at the attachment line - see Figure 1. This is approximately equal to the displacement thickness when there is no surface transpiration.

The natural leading edge Reynolds number, $\overline{R}$, is therefore

$$\overline{R} = \frac{V_e \eta}{\nu}$$

where V_e is the spanwise velocity at the edge of the attachment-line boundary layer. This can be related to other characteristic Reynolds numbers, e.g. for steady, incompressible, laminar flow

$$R_{\delta^*} = 1.026\overline{R}$$

$$R_{\theta_L} = 0.404\overline{R}$$

- see Gaster[8] and Pfenninger[7], and

$$C^* = \overline{R}^2$$

where C^* is the similarity parameter used by Cumpsty and Head[18].

When the attachment-line behaviour is investigated at different spanwise positions a length parameter **s** is introduced, where s is the spanwise distance under consideration (e.g. the spanwise length between the position of a trip wire and the measuring station or the spanwise length between the end of the suction surface and the measuring station). The associated non-dimensional group is then,

$$\frac{s}{\eta}$$

When surface transpiration is used, an additional group is required and this may take the form of a transpiration coefficient:

$$C_q = \frac{w(0)}{V_e},$$

where a positive value represents blowing and a negative value suction.

It follows that measurements made at any point along any attachment line under any combination of freestream unit Reynolds number and sweep angle can be compared provided that the three non-dimensional parameters $\overline{R}$, s/η, and C_q are duplicated.

3 Experimental Arrangement

3.1 The Model

Tests have been conducted on a large, swept-cylinder model, previously used by Danks[19] at Manchester University. This has a circular leading edge, faired to a "tear drop" section to prevent early boundary-layer separation and the formation of an oscillating wake. The spanwise chord is 0.813m and the leading edge radius is 0.203m. A perforated surface is made from 1.2mm thick titanium sheet, laser drilled, prior to model construction, with holes of 50μm diameter and hole-to-hole and row-to-row spacing of 400μm, shown in Figure 2. The entire drilling pattern is skewed relative to the axis of symmetry by 14°, leading to a streamwise hole separation of not less than 1600μm and, in general, an irregular pattern of holes along any flow streamline.

The titanium surface is divided into perforated and non-perforated areas to enable a range of suction conditions and distributions to be considered. A plan of the perforated areas is given as Figure 3. The regions of perforated surface are further divided into areas supplied by independent plenum chambers, shown in Figure 4, which permit the use of distributed suction. Each plenum chamber is connected, via valves and flowmeters, to a vacuum tank, which has a maximum suction capacity of approximately 3000 litres/minute. The model was mounted in the Cranfield College of Aeronautics low-speed, closed-return, wind tunnel which has a 2.44m x 1.83m working section and a maximum freestream velocity of 55m/s, as shown in Figure 5.

3.2 The Estimation of Flow Parameters

The accurate determination of the characteristic, leading-edge, Reynolds number is of critical importance. However, in previous investigations (e.g. Pfenninger[7] and Gaster[8]) accuracy was compromised by two issues: (i) the use of an empirical blockage correction to calculate the freestream velocity and, hence, the attachment-line velocity and (ii) the use of the geometric (measured) sweep angle. The method used in these experiments involves neither the use of a blockage correction nor the measurement of the sweep angle (except for reference).

At low freestream Mach numbers, the effects of compressibility can be neglected and Bernoulli's equation is applicable outside the boundary layers. Knowing the empty tunnel calibration (i.e. the relation between the static pressure difference across the contraction cone and the working section dynamic pressure with no model in place) and the static pressure at the start of the working section, the freestream total pressure is known. Hence, by measuring the static pressure on the attachment line, the local dynamic pressure can be calculated and, therefore, the local, attachment-line, edge velocity, V_e.

i.e.,

$$V_e = \left[\frac{p_{T_\infty} - p_a}{\frac{1}{2}\rho_\infty} \right]^{\frac{1}{2}}$$

or,

$$V_e = \left[\frac{(q + p_s)_\infty - p_a}{\frac{1}{2}\rho_\infty} \right]^{\frac{1}{2}}$$

The arrangement of the model in the working section is shown in Figure 5. It was aligned with the freestream flow by using the static pressure distribution around the leading edge of the model as a yaw meter. There are three sets of static tappings on the model (440mm, 1360mm, and 2260mm from the upstream tip). The top and bottom sets each extend to 85° either side of the line of geometric symmetry in steps of 5°. The middle set extends from 15° to 85° on one side of the model (see Figure 3). When the model is correctly aligned the static pressure coefficient distribution at any spanwise point is symmetric about the attachment-line. Figure 6 shows a typical aligned and untwisted distribution. By comparing the pressure distributions around the top, middle, and bottom of the leading edge, any yawing or twisting of the model is apparent and the alignment with the freestream can be set accurately. The static pressure distribution can also be used to determine how close conditions are to the infinite-swept ideal. Figure 6 shows that the pressure distributions at the middle and bottom tappings are in good agreement but the distribution at the top location is larger by approximately 17% at the attachment-line (x/C=0). It can be inferred from this that effectively infinite swept conditions are reached at some point between the top and middle tappings. A further experiment was performed to determine this location more precisely and it was found that effectively infinite-swept conditions were reached between 560mm and 850mm from the upstream tip.

Once the model has been aligned the chordwise velocity gradient at the attachment-line, the chordwise velocity grandient, $(dU_e/dx)_{x=0}$ can be found from the same static pressure measurements.

From Bernoulli's equation, the attachment-line, static pressure and the static pressure at any chordwise position can be related:

$$p_{T_\infty} = p_{al} + q_{al} = p_\infty + q_\infty$$

Expanding the dynamic pressure terms and re-arranging

$$p_{al} - p_\infty = \frac{1}{2}\rho\left(Q_\infty^{\,2} - V_e^{\,2}\right)$$

and so

$$p_a - p_s = \frac{1}{2}\rho U_e^2$$

This is only the case for infinite-swept conditions where $V_e = V_\infty$.

Therefore, the chordwise velocity distribution around the leading edge of the model can be determined. The chordwise velocity is non-dimensionalised using the empty tunnel freestream velocity, $\overline{Q}_\infty$, and the chordwise surface distance using the chord, C. The empty tunnel freestream velocity is used because this can be determined accurately from the empty tunnel calibration. In the region near to the attachment-line the relationship between $U_e/\overline{Q}_\infty$ and x/C is linear and the gradient can be determined by a least-squares method. This quantity will be called the divergence coefficient here and is defined as

$$C_{div} = \left[\frac{d\left(U_e/\overline{Q}_\infty\right)}{d\left(x/C\right)}\right]_{x=0} = \left[\frac{dU_e}{dx}\right]_{x=0} \cdot \left[\frac{\overline{Q}_\infty}{C}\right]$$

Note that C_{div} is independent of the freestream velocity and is dependent on the model geometry and the sweep angle. Therefore, for a given model the divergence coefficient is a characteristic of the sweep angle only. The chordwise velocity gradient is therefore,

$$\left[\frac{dU_e}{dx}\right]_{x=0} = \left[\frac{d\left(U_e/\overline{Q}_\infty\right)}{d\left(x/C\right)}\right]_{x=0} \cdot \frac{\overline{Q}_\infty}{C} = C_{div} \cdot \left[\frac{\overline{Q}_\infty}{C}\right]$$

An example of this method applied to the top pressure tappings is shown in Figure 7.

3.2.1 Data Acquisition

For each test point, tunnel static pressure, tunnel dynamic pressure and attachment-line static pressure were recorded digitally using Setra differential pressure transducers. An in-house Windows™ data acquisition package sampled the analogue outputs of the three transducers simultaneously, at 200Hz, and recorded the average of 50 samples. Ambient pressure and working section temperature were also recorded.

The output from the hot-wire was sampled using Dantec software at 60kHz. This provided ample resolution in the 0-15kHz range required.

3.3 Potential Flow Solution

For an infinite-swept, circular cylinder in incompressible, inviscid flow the pressure distribution is given by

$$C_P = \cos^2 \Lambda \left[1 - 4 \sin^2 \left(4 \frac{x}{C} \right) \right]$$

where Λ is the sweep angle. It follows that the chordwise velocity distribution is

$$\frac{U_e}{U_\infty} = 2 \sin \left(4 \frac{x}{C} \right)$$

and, hence, the chordwise velocity gradient at the attachment-line is found to be

$$\left(\frac{dU_e}{dx} \right)_{x=0} = \frac{2U_\infty}{r}$$

where **r** is the radius of the cylinder. Therefore, the divergence coefficient is

$$\left[\frac{d\left(U_e / Q_\infty \right)}{d\left(x / C \right)} \cdot \right]_{x=0} = \left(\frac{2C}{r} \right) \cos \Lambda$$

This solution is compared with the experimental results in Figure 8. For values of x/C up to ±0.3 the experimental chordwise velocity distribution at the bottom tappings is almost identical to the potential flow solution, whereas the results from the top tappings are lower. This is further evidence that infinite swept conditions are established between the top and middle tappings.

A wide range of sweep angles was used during the experimental work and, at each value, the divergence coefficient was calculated. Coefficients from the top and bottom pressure tappings are compared with the potential flow solution in Figure 9. It can be seen that the potential flow results agree well with the divergence coefficients obtained from the bottom pressure tappings throughout the sweep angle range and that the coefficients from the top tappings are significantly different from the potential flow values. Data for the bottom tappings are not available for angles below 55°, because the bottom tappings were not in the working section. For these cases, the potential flow divergence coefficient was used.

4 Cross-Flow Transition

As a result of the rapid development of the jet engine in the late 1940's, the flight envelope of aircraft increased greatly. As cruise speeds reached the transonic range, shock-wave effects began to limit the performance of straight wings and wing sweep was used to delay the onset of these effects. Flight tests on an Armstrong Whitworth 52[20], which had been designed to have laminar flow up to 60% chord on the upper wing, failed to find any laminar flow on the outboard part of the wing and further tests were authorised to investigate the effects of sweep on the stability of the laminar boundary layer. During flight tests on a variety of swept wing aircraft examined by Gray[1,2] in 1952 , transition due to cross-flow instability was discovered. Using sublimation and china-clay flow visualisation techniques, striations were observed in the laminar boundary layer prior to transition and Gray noted the similarity between the patterns observed in his tests and those caused by Görtler vortices during experiments on a cusped, unswept, aileron at NPL[21]. He also found that as sweep angle increased beyond 20°, the transition front moved swiftly towards the leading edge and, at larger angles, transition occurred at the leading edge itself. He suggested the presence of a 'cross flow' within the boundary layer, perpendicular to the external streamline, as the source of the instability.

Cross-flow instability was demonstrated theoretically by Owen and Randall[3,4] and Stuart[5], who found that, at the leading edge of a swept wing, the boundary layer velocity profile normal to the external streamline contained a point of inflexion and was, therefore, dynamically unstable[22]. This instability takes the form of stationary vortices appearing within the laminar boundary layer roughly aligned with the external flow direction which gave rise to the striation pattern which had been observed in flow visualisation. Owen and Randall proposed a cross-flow Reynolds number, χ , which depended on the characteristics of the cross-flow velocity profile and suggested that transition would occur when this Reynolds number exceeded a critical value. They estimated this to be 125 for the appearance of striations and 175 for the transition front to have moved very close to the leading edge. Stuart investigated the stability problem in three-dimensional incompressible flows, neglecting curvature effects, including a comparison between the three-dimensional cross-flow instability and Görtler type vortices. He found that, although the two conditions appeared visually similar, they were different mechanisms.

At the same time cross-flow instability was investigated experimentally on a swept wing by Anscombe and Illingworth[6] and on a swept wing and a rotating disc by Gregory and Walker[5] . Both groups noted striations in the laminar boundary layer prior to transition and that increasing sweep caused the transition front to move towards the leading edge until transition occurred very close to the leading edge. Further experimental work by Allen and Burrows[23] and Burrows[24] produced results which were in qualitative agreement with Owen and Randall's constant χ theory and work by Boltz *et al*[25] found values of χ for transition onset to be between 190 and 260. Although these were substantially higher than the value of 175 suggested by Owen and Randall, the discrepancy was blamed on the measuring techniques used and the boundary layer calculation method employed, which were approximate integral methods.

In 1961, Brown[26] extended Stuart's analytical work on stability by using a numerical method developed at Northrop that enabled the eigenvalue approach of Lin[27] to be used. Results for several three-dimensional boundary layers were presented, but is the result for the boundary layer on a swept wing with surface suction is particularly interesting. Although no quantitative data on the suction type or distribution is given, the use of suction greatly increases the critical Reynolds number for instability. Also, he showed that the greater the suction the greater the Reynolds number difference between the first appearance of the cross-flow instability and transition onset.

In 1963, Handley Page and Northrop Norair independently produced swept wings designed to have full chord laminar flow, incorporating suction systems to delay the onset of the cross-flow instability. However, in flight tests, it was found that laminar flow only occurred in small regions near the wing tips. The problem was quickly identified as attachment-line contamination and studies were launched to find a cure. Several methods were proposed, including bumps to create a stagnation point and suction to control the boundary layer. Following these, NASA flight tested the X-21 aircraft and achieved almost 100% laminar flow over the upper surface using full chord slotted suction surfaces up to chord Reynolds numbers of approximately 20×10^6.

Following the oil crisis of the early 1970's, interest in laminar flow returned as inflated oil prices increased airline Direct Operating Costs and methods of reducing overheads were sought. NASA resumed laminar flow research in 1976 as part of the Aircraft Energy Efficiency Program (ACEE) and later as the NASA Research and Technology Base Program. In 1978, Poll[28] conducted a thorough investigation of the effect of sweep on cross-flow instability. Using a swept-cylinder model, he examined the stability of the chordwise flow in the vicinity of the attachment-line at sweep angles between 52.5° and 72° using three measurement techniques: oil flow visualisation, hot-wire anemometry and surface Pitot tube. He found that the conditions at which cross-flow vortices first appeared (calculated at the position the characteristic streaks started in oil flow) could be correlated by a constant value of the cross-flow Reynolds number, χ (for a definition see Section 5) and that the value was approximately 220. He noted that, when a sublimation flow visualisation technique was used - as had been the case in previous investigations, a lower value of χ was obtained for the first appearance of striations. However, when correlating the data for the onset of transition, Poll showed that χ varied with chordwise position and that the constant χ hypothesis was of limited value.

Two types of vortex occur in three-dimensional boundary layers due to cross-flow instability: stationary vortices and travelling vortices. The type which dominates transition has been linked to the receptivity mechanism of the boundary layer in work by Bippes and Müller[29] and Bippes[30], using wind tunnels with different freestream turbulence intensities. In the high turbulence conditions, they found that travelling cross-flow vortices were observed, whereas, in the low-turbulence environment, stationary vortices were dominant. Linear, stability theory predicts that travelling cross-flow disturbances are amplified more rapidly than stationary ones, but work by Kohama *et al*[31] showed that the transition process is dominated by a high frequency, secondary instability rather than the primary, low frequency instability. This secondary instability, with a frequency an order of magnitude larger than the primary instability, is caused by the parallel, co-rotating stationary vortices near the edge of the boundary layer. High

momentum fluid is bordered by low momentum fluid, which leads to multiple inflection points high in the streamwise velocity profiles (Poll[28] noted a high frequency instability during his work which may have been the first observation of the secondary instability). This process is highly non-linear. Saric *et al*[32] showed that the intermittency of stationary cross-flow vortices is strongly influenced by streamwise vorticity and that, even in the Stokes-flow limit, a small three-dimensional roughness is a source of vorticity. Further work on micron-sized roughness elements[33] showed that the effect of isolated 6μm roughness elements was confined to a small chordwise zone close to the attachment-line where the cross-flow disturbances were first amplified and that transition was caused by the stationary vortex which passed close to the location of the roughness element.

Computational work by Malik *et al*[34] attempted to demonstrate the dominance of the stationary cross-flow vortex and the appearance of a high frequency secondary disturbance. The swept Hiemenz flow which forms near an attachment-line was used and both linear and non-linear PSE calculations were performed. Good correlation was obtained with experimental results. The wall vorticity distribution showed the streaks (or striations) associated with the onset of cross-flow instability and the multiple inflection points in the streamwise velocity profiles of the stationary cross-flow vortices were found. High frequency secondary instability was also present and had a frequency an order of magnitude larger than the most amplified travelling mode, in agreement with the findings of Kohama and Poll.

Radeztsky[35] compared linear stability results from previous investigations with detailed measurements taken for the growth of low amplitude stationary cross-flow vortices. Linear theory correctly predicted the mode shapes and the wavelengths of the cross-flow vortex, including the most amplified wavelength. However, the growth rates were not well described and, in many cases, theory predicted strong growth when, in experiment, the amplitude was actually decaying. Taken in conjunction with results from Bippes[30] and Dagenhart[36], it can be seen that linear theory fails to predict the correct growth of cross-flow vortices, even when curvature and non-parallel effects are included. Reibert *et al*[37] reported a comparison with non-linear PSE calculations and showed good correlation for the growth rate of the cross-flow vortex.

Danks[19] studied the effect of suction on transition at, and near, a swept attachment-line using a swept-cylinder model. He found that modest amounts of suction could be used to delay the onset of cross-flow instability, at least until the minimum pressure location on his model, provided transition was caused by cross-flow instability and not attachment-line contamination. The porous surface was supplied by eight plenum chambers (see Figure 4), so that different distributions of suction could be used. He found that there was no single, most effective, suction distribution, but that a number of successful distributions had approximately the same average suction coefficient. It was also found that suction was not required through all the plenum chambers round to the monitoring station. Suction was most effective when applied close to the attachment-line. Danks noted that suction applied off the attachment-line could be used to relaminarise a chordwise boundary layer which had been contaminated by a turbulent attachment-line. Again, various suction distributions were used and it was found that, for transition at the minimum pressure location, the average suction

coefficient required was an order of magnitude larger than had been required for the situation with no attachment-line contamination.

Bippes and Lerche[38] investigated the effect of suction on travelling and stationary cross-flow vortices on a swept, flat plate. On a porous surface, without suction, the amplitudes of both travelling and stationary disturbances were more than double those on a polished non-porous surface at the same conditions. When suction was applied the amplitudes of travelling disturbances were damped, but the amplitudes of stationary disturbances were unaffected or even slightly increased. This is very surprising in light of Danks' results, but the authors claimed this was due to considerable non-uniformity of the suction velocity across the plate due to manufacturing quality. However, no details of the suction used (distribution or magnitude) were given so firm conclusions cannot be drawn.

5 Natural Cross-Flow Transition

Owen and Randall[3] suggested that a suitable Reynolds number for the study of cross-flow instability, χ, might be

$$\chi = \frac{\bar{v}_{max}\delta}{\nu}$$

where $\bar{v}_{max}$ is the maximum value of the cross-flow velocity and δ is the boundary-layer thickness. They also suggested that the onset of transition could be correlated by a constant value of χ. Poll[12] redefined the cross-flow Reynolds number, in a more precise manner, as

$$\chi = -\frac{\bar{v}_{max}\,\Delta}{\nu}$$

where $\bar{v}_{max}$ is the maximum value of the cross-flow velocity and Δ is the height above the surface at which the cross-flow velocity drops to 1% of its maximum value. This is easy to calculate using numerical boundary layer methods and provides an unambiguous method for determining χ. He showed that, for the onset of transition, the constant χ hypothesis was incorrect and that χ varied with chordwise position, x/C, as well.

Assuming incompressible flow and an adiabatic wall, the flow in the immediate vicinity of a swept attachment-line can be determined from $(dU_e/dx)_{x=0}$, V_e, the chordwise position, x, the freestream viscosity, μ, and the freestream density, ρ. Locally, the chordwise velocity, U_e, is

$$U_e = \left(\frac{dU_e}{dx}\right)_{x=0} .x$$

According to Buckingham's π theorem, five physical variables involving three fundamental dimensions can be re-expressed as two non-dimensional π products. It is convenient to choose these as the leading edge Reynolds number, $\overline{R}$, and the chordwise Reynolds number, Re_x, where

$$Re_x = \frac{U_e\,x}{\nu} = \frac{\left(dU_e/dx\right)_{x=0} x^2}{\nu}$$

Danks[19], using Poll's data along with some of his own, showed that these two parameters collapsed the data for the onset of transition and those for the end of transition onto single curves. These are shown in Figure 10. From this it can be seen that it is not necessary to calculate the cross-flow Reynolds number, χ, for this simplified situation.

5.1 Objectives

The transition that occurs due to cross-flow instability on a non-porous surface will be studied and compared with Poll's work, both as a benchmark exercise and to confirm the dimensional analysis outlined above. Natural transition on a porous surface without suction will then be examined to determine the effect of porosity on the cross-flow instability.

5.2 Experimental Method

The arrangement of the model in the wind tunnel is shown in Figure 5. For these tests the top half of the model, i.e. that portion between the top and middle static pressure tappings, was used and the distribution of porous and non-porous regions on this part of the model is shown in Figure 3. Measurements were taken with sweep angles ranging from 45° to 70° and the state of the boundary layer was monitored by a hot-wire anemometer placed 1300mm from the upstream tip of the model. The hot-wire filament was set as close to the surface of the model as possible and the reflective surface made it possible to set the height to less than 1mm. Chordwise positions between x/C=0.142 and x/C=0.231 were used and, for each case, the freestream velocity was increased until the onset of transition occurred. The conditions were then noted.

For the measurements on the porous surface, the suction system was shut off so that no net transpiration occurred and, for each test, the plenum chamber pressures were allowed to stabilise before the transition conditions were recorded. It should be noted that the porous surface began at x/C=0.044 and not at x/C=0. This was because the porous surface had been fabricated so that the attachment-line and cross-flow transition mechanisms could be studied entirely separately.

5.2.1 Transition Onset Criterion

The first indication of cross-flow instability was usually, although not always, the appearance of a harmonic, laminar disturbances that were similar to T-S waves when viewed on an oscilloscope. The onset of transition was indicated by turbulent bursts and onset was deemed to have occurred when between one and three turbulent bursts passed the hot-wire location every two seconds. Care was taken to ensure that the criterion was fulfilled for a reasonable time period (between two and three minutes) before values were recorded. Examples of the hot-wire signals and power spectra for the stable laminar boundary layer are shown in Figures 11 and 12, the unstable layer in Figures 13 and 14, the onset of transition in Figures 15 and 16 and for fully turbulent flow in Figures 17 and 18. In general, the amplitude of the laminar disturbance increased with increasing chordwise position and, at times, was of the same order of magnitude as the turbulent bursts.

5.3 Results and Analysis

5.3.1 Non-Porous Surface

The results are shown in Figure19, with the data from Poll[12] and Danks[19] for comparison. For clarity, the data from Poll and Danks has been reduced to a best-fit line with error bars to show the scatter of the data. The agreement is excellent and this justifies the use of $\overline{R}$ and Re_x to describe cross-flow transition in the region near the attachment-line. It is important to note that the results are independent of the method used to monitor the boundary layer, since Poll used both hot-wire anemometry and surface Pitot tubes during his work. At high $\overline{R}$, attachment-line contamination becomes the dominant transition mechanism and this can be seen on Figure 19 as an upper limit on $\overline{R}$. The only difference between the current work and that of Poll is the value of $\overline{R}$ at which this occurs. From Poll, this is approximately 700 as compared with 750 here. This is due to the fact that smaller s/η values were used in the current tests and this is entirely consistent with Poll's work on transition at the attachment-line in the absence of a trip wire[28].

5.3.2 Porous Surface

The effect of a porous surface was examined by comparing conditions on the two sides of the model at the same chordwise positions relative to the attachment-line. Results are shown in Figure 20 and it is immediately apparent that the porous surface causes a reduction in the Reynolds numbers required for the onset of transition. This is in qualitative agreement with the results from Bippes and Lerche[38]. They found that the effect of a porous surface, on a swept flat-plate model, was to increase the amplitude of both travelling and stationary disturbances compared with equivalent conditions on a polished, non-porous surface. Figure 21 shows the change in $\overline{R}$ as Re_x increases. The reduction in $\overline{R}$ increases until an Re_x of about $4x10^5$ and then remains approximately constant at 57. Expressing this reduction as a percentage of the $\overline{R}$ for transition onset on a non-porous surface, ie

$$\% \text{ reduction} = \left(\frac{\overline{R}_{porous} - R_{non-porous}}{\overline{R}_{non-porous}} \right) x100$$

The percentage reduction increases with Re_x, from 8% at an Re_x of $1x10^5$ to 14.5% when Re_x reaches $1x10^6$, as shown in Figure 22. This shows that as Re_x increases the destabilising effect of the porous surface increases, since at lower $\overline{R}$ it would be expected that the flow would be more stable to the amplification of small disturbances. Therefore, Re_x could be viewed as a measure of the amplification of the cross-flow instability (i.e. the larger Re_x the greater the amplification rate of the cross-flow instability and the lower the value of $\overline{R}$ for the onset of transition).

The data for the onset of transition on both porous and non-porous surfaces can be represented by power laws. These are given below and are shown in Figure 23, together with the experimental data.

For $100\text{x}10^3<\text{Re}_x<1000\text{x}10^3$

Onset of transition on a non-porous surface: $\overline{R} = 29400\,\text{Re}_x^{-0.31}$

Onset of transition on a porous surface: $\overline{R} = 57400\,\text{Re}_x^{-0.37}$.

Therefore, the change in $\overline{R}$ due to the porous surface is

$$-\Delta\overline{R} = 29400\,\text{Re}_e^{-0.31}\left(1.95\,\text{Re}_x^{-0.06} - 1\right)$$
$$\text{for } 100\text{x}10^3<\text{Re}_x<1000\text{x}10^3$$

This is compared with the measured reduction in $\overline{R}$ in Figure 24.

5.4 Implications

To implement Hybrid Laminar Flow Control (HLFC) a surface through which air can be drawn is required. This can be either slotted, drilled or naturally porous. Using modern manufacturing methods, surfaces with small waviness and roughness can be produced relatively easily and the laser or electron-beam drilling processes can produce surfaces with very small holes spaced and arranged as required. Assuming that a drilled surface is used, it appears that holes, acting as distributed roughness, cause the onset of transition to occur at a lower values of the characteristic Reynolds numbers than would be the case for a smooth non-porous surface.

How might this affect a large aircraft in cruise? From Poll[28], for a Boeing 727 in cruise, $\overline{R}$ is approximately 560. For this aircraft, fitted with a porous surface, identical to the one used here, transition due to cross-flow instability would occur at an Re_x value of 274400, compared with 364420 for the solid surface - a reduction of 25%. Therefore, the obvious next question is ***how much suction is required to bring the Reynolds numbers for the onset of transition back to those for a non-porous surface?*** Clearly, there is a price to be paid for the use of a perforated surface, even before suction is used to delay transition.

6 The Control of Cross-Flow Instability By Surface Suction

Very little experimental work has been done on the effect of suction on cross-flow instability. Bippes and Lerche[38] investigated the effect of suction on travelling and stationary waves individually. They found that suction damped travelling waves but had little effect on stationary waves, although no details of the suction amount or distribution were given. Danks[19] studied the effect of the suction distribution qualitatively. Although no parametric trends were identified, he found that suction applied close to the attachment-line was more effective than that applied at larger chordwise positions. For transition at the minimum pressure location (x/C=0.349), Danks found that the most efficient average suction coefficient was approximately 0.00034 and that suction was not necessary at values of x/C greater than 0.25.

6.1 Objectives

The effect of uniform, distributed suction on the transition that occurs due to cross-flow instability will be studied quantitatively and compared with the natural transition on porous and non-porous surfaces.

6.2 Experimental Method

The arrangement of the model in the wind tunnel was the same as that for the previous tests. As with the natural transition experiments, measurements were made on the top half of the model. To apply uniform, distributed suction, the porous surface was supplied by eight plenum chambers, so that the external, surface static pressure variation over each chamber (in the chordwise direction) was small. The porous region extended from 10° to 90° (x/C=0.044 to x/C=0.393), with each plenum chamber supplying a 10° segment of surface. Porosity was not used around the attachment-line (0° to 10°) so that attachment-line transition and cross-flow instability could be studied entirely separately. With this arrangement, the flow around the chord would not be affected by the roughness of the porosity on the attachment-line or by any damping effect caused by suction at the attachment-line. Therefore, the conditions are probably not representative of a typical HLFC wing in service, where attachment-line suction maybe necessary to control contamination from the turbulent fuselage boundary layer and transition due to roughness effects (e.g. inset impact, steps and gaps, waviness, etc.). However, uniform, distributed suction is a very useful benchmark, with the reduced number of variables allowing a thorough investigation.

Suction was applied by connecting the plenum chambers, via a set of rotameter flowmeters and valves, to a pair of large capacity evacuation tanks. The size of the tanks, combined with evacuation pumps which were run during the experiments, meant that the overall suction pressure (the pressure difference between the vacuum tanks and the plenum chambers) during any test was essentially constant. The flowmeters

measured the volumetric flow-rate and were calibrated using the flowmeter outlet static pressure. Each flowmeter was equipped with a valve, so the volumetric flow-rate through each plenum chamber could be set accurately. In addition, each plenum chamber had three static pressure ports, distributed in the spanwise direction, so the internal plenum static pressure and pressure distribution could be monitored. The plenum static pressure could not be used to calculate the volumetric flow-rate accurately, for reasons described by Danks[19], but it could be used to give an approximate value for the flow-rate which could be checked against the value deduced from the flowmeter. This was an excellent method for spotting and checking for leaks in the suction system. The plenum static pressures were also used to check the internal static pressure distribution of the plenum chamber to ensure that uniform distributed suction was applied within the chamber.

Measurements were taken with sweep angles ranging from 45° to 70° and, at each, the state of the boundary layer was monitored by a hot-wire anemometer placed 1300mm from the upstream tip of the model. The hot-wire filament was set as close to the surface of the model as possible. Chordwise positions between x/C=0.142 and x/C=0.231 were used and the freestream velocity was increased until the onset of transition occurred. For each point, the pressures within the plenum chambers were allowed to stabilise before the conditions were noted. The attachment-line boundary was monitored at all times, so that transition due to attachment-line contamination could not be mistaken for that due to cross-flow.

6.2.1 Transition Onset Criterion

The first appearance of cross-flow instability was usually, although not always, in the form of harmonic laminar disturbances visually similar to T-S waves. Transition onset was indicated by turbulent bursts and onset was deemed to have occurred when between one and three turbulent bursts passed the hot-wire location every two seconds. Care was taken to ensure that the criterion was fulfilled for a reasonable time period (between two and three minutes) before values were recorded.

6.3 Results and Analysis

The results are plotted in Figure 25. In order to produce readily interpretable information, the raw data were interpolated to give results at specific values of the suction coefficients. Data for zero C_q are for the onset of transition on a porous surface, as described previously (Section 5.2.3) and Poll's data for the onset of transition on a non-porous surface have been included for comparison.

It is immediately apparent that suction can be used to control transition due to cross-flow instability. The data form a series of 'stacked' curves of similar shape and the results for each suction coefficient can be described by a simple power law, as could the 'natural' transition results discussed previously. The scatter of the data increases as the suction coefficient increases, but the agreement with the data for C_q values of 0, -

0.00006, and -0.00012 is good so the method has been extended to the larger coefficients. It is important to note that the curves are not parallel. They are closer to each other at large Re_x, which implies that the effect of suction decreases with increasing Re_x. The form of the power law used to model the data was changed slightly to include this. Previously the power law used was

$$\overline{R} = A\,Re_x^{\,n}$$

where **A** and **n** were constants. This was changed to

$$\overline{R} = A\,Re_x^{\,n} - \left(BC_q\,Re_x\right)$$

where B is constant. In this way, increasing Re_x would reduce the $\overline{R}$ for transition onset. For simplicity, and entirely arbitrarily, the constant A was set to the same value as for the natural, transition on a porous surface (i.e. C_q=0). Empirical curve fits were then found for C_q's of -0.00006, -0.00012, -0.00018 and -0.00024, since these data sets had the least scatter. The results are shown in Figure 26, together with the experimental data and the agreement is good. The variation of **n** and **B** with suction coefficient was then examined. Both vary almost linearly with C_q, as shown in Figures 27 and 28. From these, a relation can be determined which describes the variation of $\overline{R}$ and Re_x with C_q, i.e.

$$\text{for } 200\text{x}10^3 < Re_x < 1100\text{x}10^3 \text{ and } -0.00018 < C_q < 0$$

$$\overline{R} = 57400\,Re_x^{\,-(95C_q+0.37)} + \left[0.25\,Re_x\,C_q\right].$$

Curve fits were then generated for C_q of -0.0003 and -0.00036, the data sets which were not used to develop the relation. A comparison between these experimental data and the approximations is shown in Figure 29. Despite the scatter, it can be seen that the curve fits are entirely satisfactory for

$$200\text{x}10^3 < Re_x < 1100\text{x}10^3 \text{ and } -0.00036 < C_q < 0.$$

6.4 Implications

It has been shown that the onset of transition due to cross-flow instability can be delayed by suction through a porous surface in the region near the attachment-line. Also, the reduction in the natural transition $\overline{R}$ caused by the porous surface can be eliminated by using suction. However, the effect of suction depends upon the

chordwise Reynolds number, Re_x and is less effective at large Re_x. If we assume that Re_x can be used as a rough guide to the amplification rate of the cross-flow disturbances i.e. more amplification at larger Re_x then the reduction in the effectiveness of suction with increasing Re_x is to be expected.

7 The Effect of Two-Dimensional Disturbances on Cross-Flow Induced Transition

Two-dimensional, trip-wires are commonly used in boundary layer studies as a simple method of introducing "controlled" disturbances. The effect on flat-plate boundary layers has been investigated thoroughly, in particular Gibbings[39,40] and Hall[41]. The effect of two-dimensional, trip-wires at the leading edge of a swept wing has been studied in detail by Poll[28]. He investigated the effect of varying the trip-wire diameter and varying the distance between the trip-wire and the measuring station on the attachment-line.

In the present study, the effect of two-dimensional, trip-wires on cross-flow transition was considered.

7.1 Experimental Arrangement

The same wind tunnel arrangement described previously was used. Different diameter, trip-wires were wrapped around the leading edge, perpendicular to the spanwise generators, and approximately 790mm from the upstream tip. Care was taken to ensure the wire was perpendicular to the spanwise flow, was in contact with the surface all around the leading edge, and was sufficiently tight to prevent any vibration. When a new wire was attached, the $\overline{R}$ at the onset of transition on the attachment-line was measured and compared with Poll's results to check that the wire was attached correctly. This test was repeated periodically to ensure the trip-wire had not become loose.

The state of the boundary layer was monitored at various chordwise positions, from 35° to 80°, on both the non-porous and porous surfaces. A hot-wire anemometer was placed 1350mm from the upstream tip (this position corresponded to the end of the porous surface on one side of the model). The non-porous surface was tested at 60.4° sweep with trip-wires of diameter 0.21mm and 0.34mm. The porous surface was tested at 60.4° and 63.8° with trip-wires of diameter 0.21mm and 0.268mm.

During tests on the porous surface all of the suction system hoses were closed and sufficient time was left for the pressures inside and outside the plenum chambers to equalise before measurements were taken.

7.1.1 Transition Onset Criterion

The onset of transition was indicated by the regular appearance turbulent bursts as in the previous experiments.

7.2 Results

The results for two-dimensional, trip-wires on the non-porous surface are shown in Figure 30. It can be seen that the onset of transition with a trip coincides with that on a non-porous surface without a trip-wire, until transition at the attachment-line overrides the cross-flow transition process. Transition then occurs at a constant value of $\overline{R}$ (and therefore s/η). This is consistent with Poll's results for the onset of transition at the attachment line, if the distance, s, is taken to be the distance between the trip and the spanwise position of the hot-wire. Natural transition characteristics on the porous surface are shown in Figure 31, along with the curve fit for natural transition on a porous surface without a trip-wire (i.e. $\overline{R} = Re_x^{-0.37}$). Although there is some scatter, it appears that the onset of transition on a porous surface with a two-dimensional trip agrees with the data for a porous surface without a trip. Therefore, cross-flow instability is not affected by two-dimensional, trip-wires set normal to the spanwise generators, whether the surface is porous or not.

7.2.1 Two-Dimensional Trips

The nature of the attachment-line flow is such that discrete fluid elements do not travel along the span. Instead, fluid is constantly moving in the chordwise direction and being replaced by new fluid entrained from the freestream. Therefore, "turbulence" must be propagated along the attachment line by a mechanism that is independent of the fluid elements themselves and is probably a system of pressure waves. For disturbance sources (e.g. two-dimensional trips) on the attachment line, this means that, whilst the perturbation introduced may be convected indefinitely along the attachment line, the fluid whose momentum has been modified will be swept away in the chordwise direction - forming a turbulent wedge attached to the source.

For the experiments described here, the spanwise distance between the trip-wire and the measuring station was sufficiently large for no momentum defect, introduced at the wire, to be detectable at the measuring station. For $\overline{R}$ values smaller than those that caused turbulent bursts on the attachment line, the disturbance caused by the trip wire but did not interact with the cross-flow instability mechanism. This agrees with work by Radeztsky *et al*[33] who used a two-dimensional, trip wire on a swept, aerofoil. They found that the cross-flow instability was only affected locally by the stationary, cross-flow vortices that originated near the ends of the trip wire.

Conclusions

Transition that occurs near a laminar, attachment line due to cross-flow instability has been investigated. It has been shown that, on a non-porous surface, the conditions at onset can be described by two non-dimensional parameters, $\overline{R}$ and Re_x. The relationship can be approximated adequately with a power law.

On a porous surface with no transpiration, transition occurs at a lower value of $\overline{R}$ than on a non-porous surface at the same Re_x. This represents a performance penalty due to the interaction of the cross-flow instability with the surface "roughness" associated with the holes and, or, the drilling process. The performance penalty for the configuration used in these experiments has been determined. However, it is probable that, in general, it is a complex function of the physical characteristics of the porous surface.

Suction has been used to delay the onset of transition and it has been demonstrated that transition due to cross-flow instability can be delayed with surface transpiration. Conditions at the onset of transition are a function of $\overline{R}$, Re_x, and C_q and a simple expression has been derived which reproduces the relation over a wide range of conditions.

The effect of two-dimensional, trip wires, set normal to the spanwise generators, on cross-flow transition has been studied. These had no effect on transition except when the trip produced a turbulent, attachment-line flow.

References

1. Gray, W E: ***The effect of wing sweep on laminar flow***. RAE Technical Memo 255, February 1952

2. Gray, W E: ***The nature of the boundary layer at the nose of a swept wing***. RAE Technical Memo 256, June 1952

3. Owen, P R and Randall, D G: ***Boundary layer transition on a swept back wing***. RAE Technical Memo 277, 1952

4. Owen, P R and Randall, D G: ***Boundary layer transition on a swept back wing: a further investigation***. RAE Technical Memo 330, 1953

5. Gregory, N and Stuart, J T and Walker, W S: ***On the stability of three-dimensional boundary layers with application to the flow due to a rotating disk***. Philosophical Transactions of the Royal Society, Series A, Vol. 248, 1955- 56, pp155-199

6. Anscombe, A and Illingworth, L N: ***Wind-tunnel observations of boundary layer transition on a wing at various angles of sweepback***. Aeronautical Research Council Reports and Memoranda No. 2968, May 1952

7. Pfenninger, W: ***Flow problems of swept low drag suction wings of practical construction at high Reynolds numbers***. Lecture Presented at Subsonic Aeronautics Meeting, New York, April 1967

8. Gaster, M: **On the flow along swept leading edges**. *The Aeronautical Quarterly*, May 1967

9. Fisher, D and Fischer, M: ***The development flight tests of the Jetstar LFC leading-edge flight experiment***. NASA Symposium on NLF and LFC Research, NASA CP-2487, pp117-140

10. Maddalon, D V and Braslow, A L: ***Simulated airline service flight tests of laminar flow control with perforated surface suction system***. NASA Technical Paper 2966, 1990

11. Nitsche, W and Szodruch, J: ***Concepts and results for laminar flow research in wind tunnel and flight experiments***. ICAS Conference Proceedings, 1990

12. Poll, D I A: **Transition in the infinite swept attachment-line boundary layer**. *The Aeronautical Quarterly*, Vol. XXX, November 1979

13. Gregory, N and Stuart, J T and Walker, W S: ***On the stability of three-dimensional boundary layers with application to the flow due to a rotating disc.*** Philosophical Transactions of the Royal Society of London, Series A, Vol. 248, pp155-199

14. Emmons, H W: **The laminar-turbulent transition in a boundary layer, part 1.** *Journal of Aerospace Sciences*, Vol. 18, 1951, pp490-498

15. Morkovin, M V: ***On the many faces of transition.*** Viscous Drag Reduction (editor C S Wells), Plenum, 1969, pp1-31

16. Morkovin, M V: ***Instability, transition to turbulence and predictability.*** AGARDograph No. 236, 1977

17. Choudhari, M and Streett, C L: ***Boundary layer receptivity phenomena in three-dimensional and high-speed boundary layers.*** AIAA 90-5258. AIAA Second International Aerospace Planes Conference, Orlando, 1990

18. Cumpsty, N A and Head, MR: **The calculation of three-dimensional turbulent boundary layers. Part II attachment-line flow on an infinite swept wing.** *The Aeronautical Quarterly*, Vol. XVIII, May 1967, pp150-164

19. Danks, M: ***Issues relating to laminar flow control on the leading edge of swept wings.*** PhD Thesis, Manchester University, June 1995

20. Gray, W E: ***Laminar flow at high Reynolds number.*** RAE Technical Memo (Aero) No. 98, June 1950

21. Gregory, N and Walker, W S: ***The effect on transition of isolated surface excrescences in the boundary layer.*** ARC Report No. 13436, October 1950

22. Tollmein, W: ***Ein allgemeines kriterium der instabilität laminarer geschwindigkeits-verteilungen.*** Nachr. Ges. Wiss. Göttingen, Math. Phys. Klasse, Fachgruppe I, 1, 79-114, 1935

23. Allen, L D and Burrows, F M: ***Flight experiments on the boundary layer characteristics of a swept back wing.*** College of Aeronautics Report No. 104, Cranfield Institute of Technology, 1956

24. Burrows, F M: ***A theoretical and experimental study of the boundary layer flow on a 45° swept back wing.*** College of Aeronautics Report No. 109, Cranfield Institute of Technology, 1956

25. Boltz, F W and Kenyon, G C and Allen, C Q: ***Effects of sweep angle on the boundary layer stability characteristics of an untapered wing at low speeds.*** NASA Technical Note D-338

26. Brown, W B: ***A stability criterion for three-dimensional laminar boundary layers.*** Boundary Layer and Flow Control (Edited by G V Lachmann), Vol. 2, 1961, pp913-923. Pergamon Press Ltd

27. Lin, C C: **On the stability of two-dimensional parallel flows.** *Quarterly of Applied Mathematics,* 177, 1945-46

28. Poll, D I A: ***Some aspects of the flow near a swept attachment-line with particular reference to boundary layer transition.*** PhD Thesis, Cranfield Institute of Technology, 1978

29. Bippes, H and Müller, B: ***Disturbance growth in an unstable three-dimensional boundary layer.*** Numerical and Physical Aspects of Aerodynamic Flows, Vol. IV (Editor T. Cebeci), Springer-Verlag, 1990

30. Bippes, H: ***Experiments on transition in three-dimensional accelerated boundary layer flows.*** Proceedings of the Royal Aeronautical Society Boundary Layer and Transition Control Conference, Cambridge, 1991

31. Kohama, Y and Saric, W S and Hoos, J A: ***A high frequency secondary instability of cross-flow vortices that leads to transition.*** Proceedings of the Royal Aeronautical Society Boundary Layer and Transition Control Conference, Cambridge, 1991

32. Saric, W S and Krutckoff, T K and Radeztsky, R H: ***Visualisation of low-Reynolds-number flow fields around roughness elements.*** Bulletin of the American Physics Society, Vol. 35, No. 2262, 1990

33. Radeztsky, R H and Reibert, M S and Saric, W S: ***Effect of micron-sized roughness on transition in swept wing flows.*** AIAA 93-0076, 31st Aerospace Sciences Meeting, Reno, 1993

34. Malik, M R and Li, F and Chang, C-L: **Crossflow disturbances in three-dimensional boundary layers: non-linear development, wave interaction and secondary instability.** *Journal of Fluid Mechanics,* Vol. 268, 1994, pp1-36

35. Radeztsky, R H and Reibert, M S and Saric, WS: ***Development of stationary crossflow vortices on a swept wing.*** AIAA 94-2373, 25th AIAA Fluid Dynamics Conference, Colorado Springs, 1994

36. Dagenhart, J R: ***Crossflow disturbance measurements on a 45-degree swept wing***. NASA TM-108650, 1992

37. Reibert, M S and Saric, W S and Carrillo Jr, R B: ***Experiments in non-linear saturation of stationary crossflow vortices in a swept-wing boundary layer***. AIAA 96-0184, 34th Aerospace Sciences Meeting and Exhibit, Reno, 1996

38. Bippes, H and Lerche, T: ***Transition prediction in three-dimensional boundary-layer flows unstable to crossflow instability***. AIAA 97-1906, 1997

39. Gibbings, J C: ***On boundary-layer transition wires***. ARC CP 462, December 1958

40. Gibbings, J C and Goksel, O T and Hall, D J: **The influence of roughness trips upon boundary layer transition, parts 1, 2 and 3**. *Aeronautical Journal*, 90 (898-900), pp289-301, 357-367, 393-398, 1986

41. Hall, D J: ***Boundary layer transition***. PhD Thesis, University of Liverpool, 1968

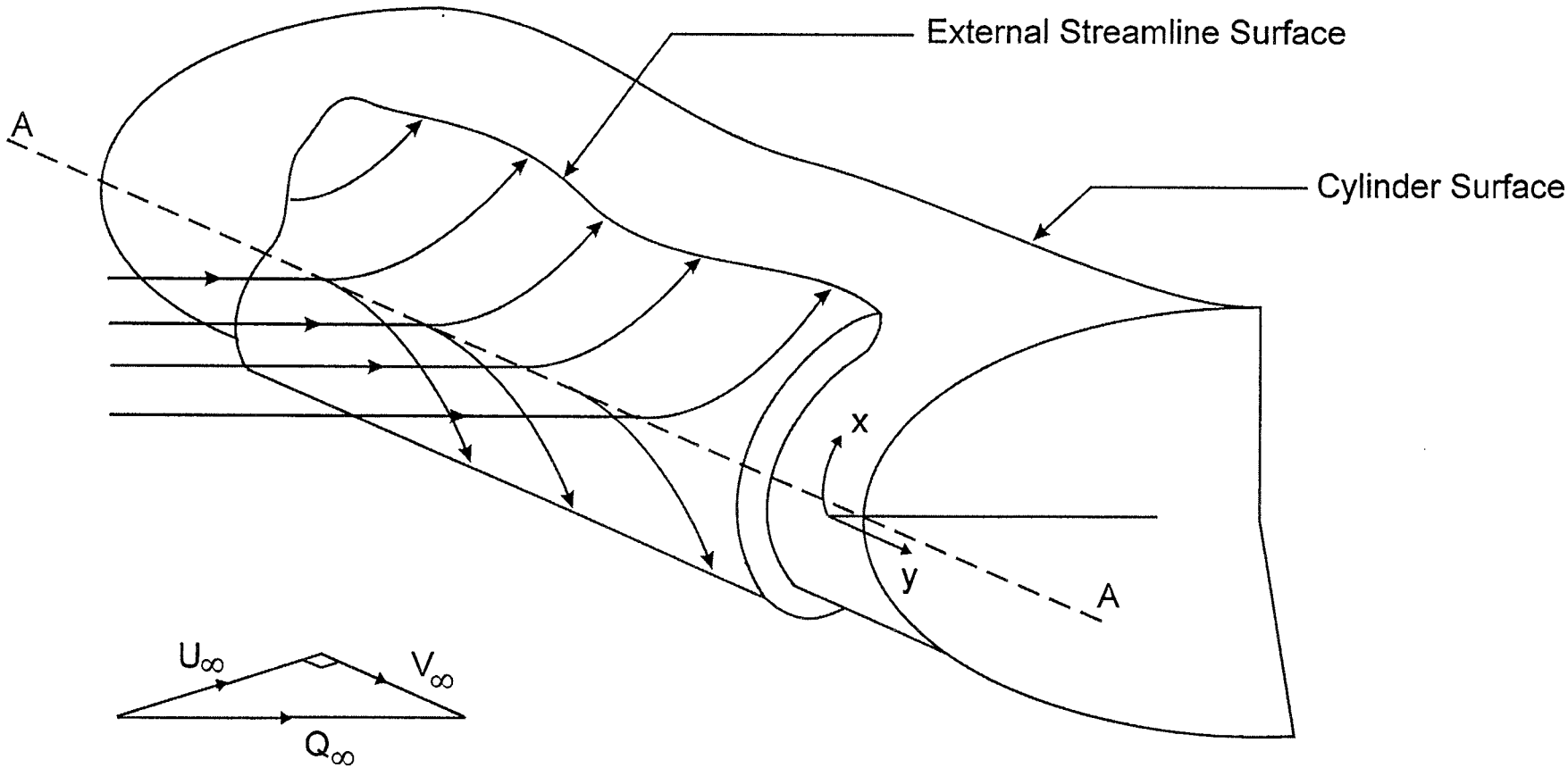

Figure 1. The Flow Near The Leading Edge of a Swept Wing

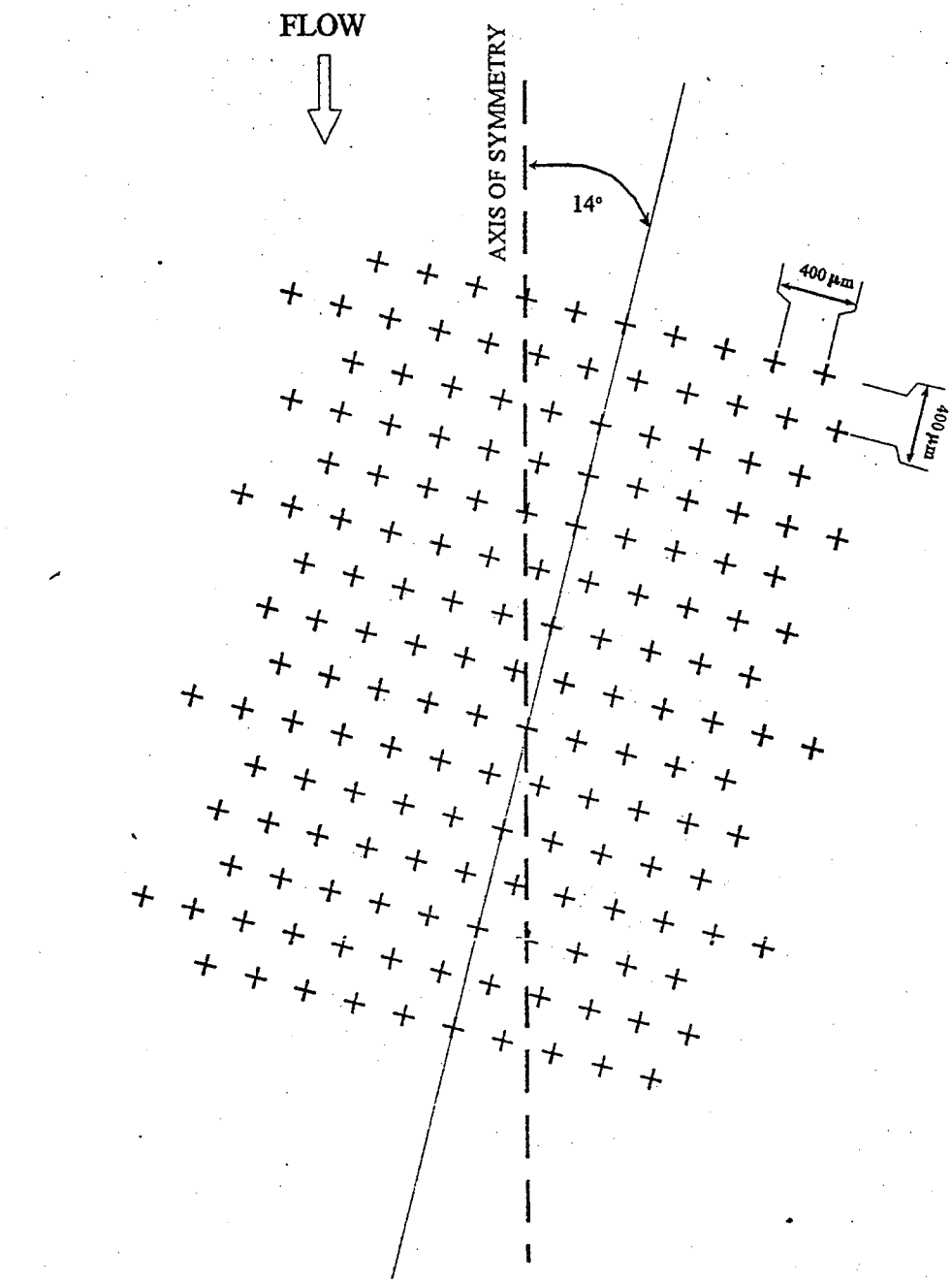

DRILLING PATTERN SHOWING
SKEW ANGLE.

HOLES DRILLED 50 microns O/D @ 400 microns PITCH

Figure 2. Leading Edge Perforation Pattern

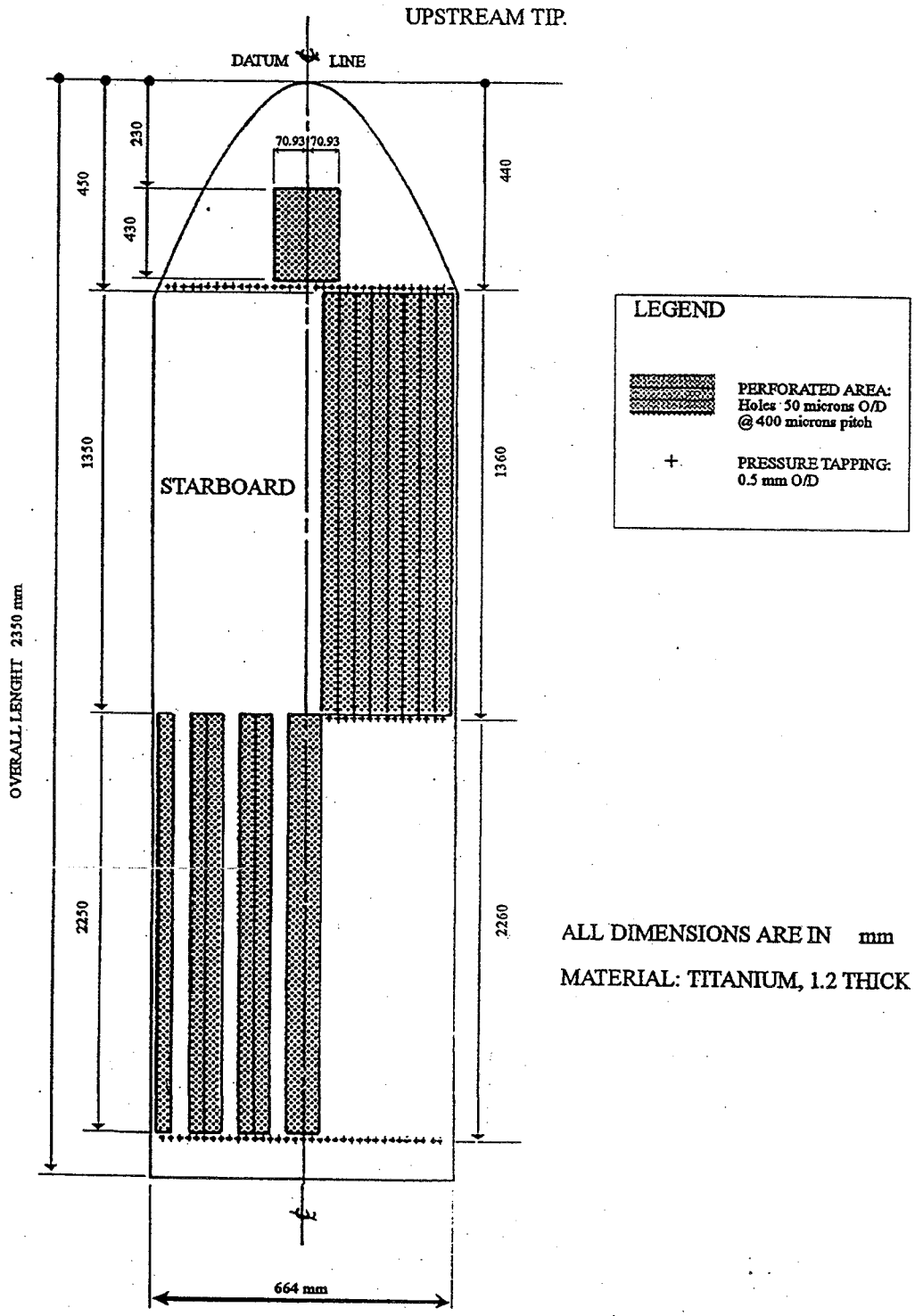

Figure 3. Distribution of Perforated Areas on The Titanium Leading Edge Panel

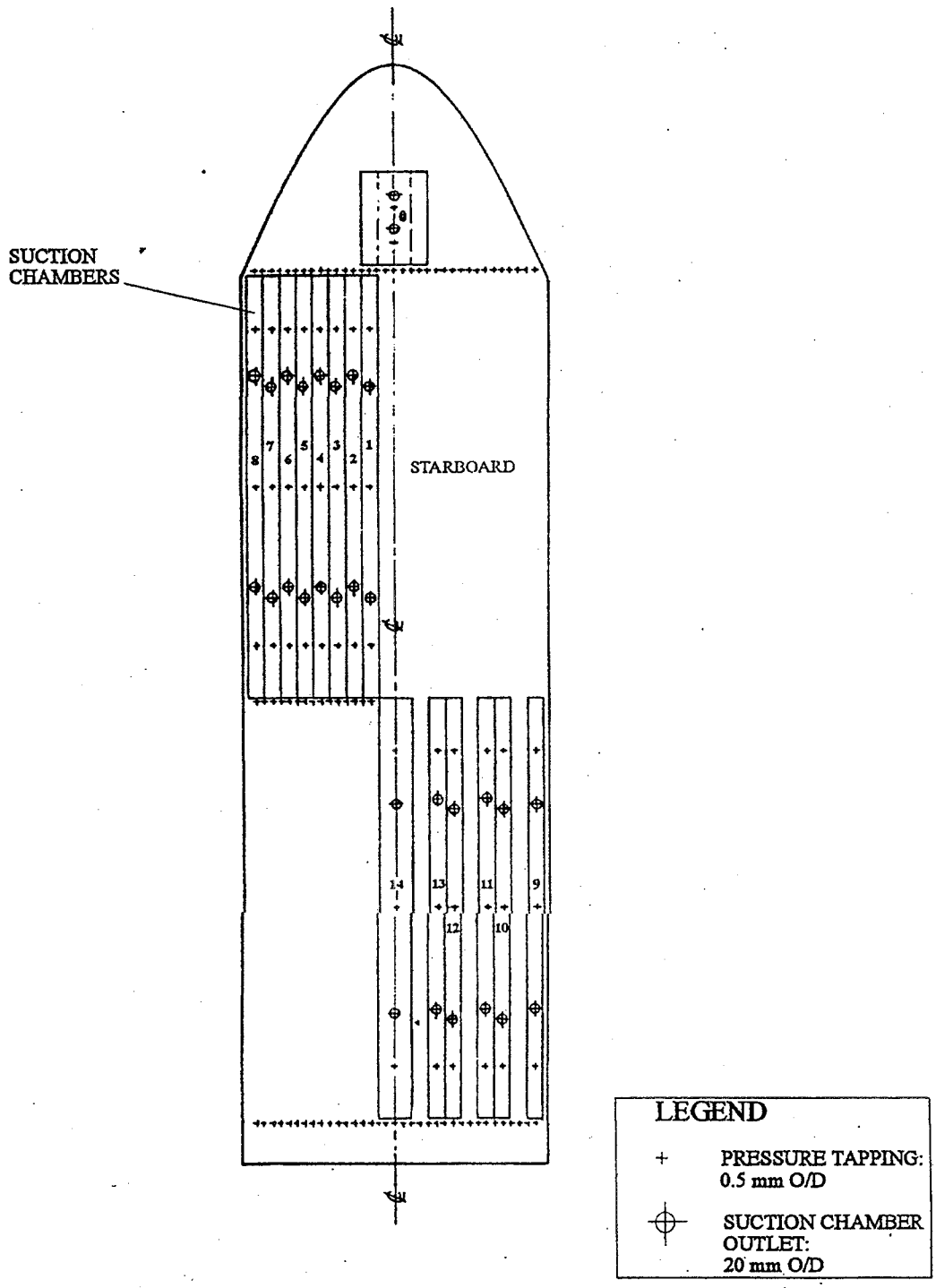

Figure 4. Distribution of Suction Chambers Within the Perforated Titanium Leading Edge Surface

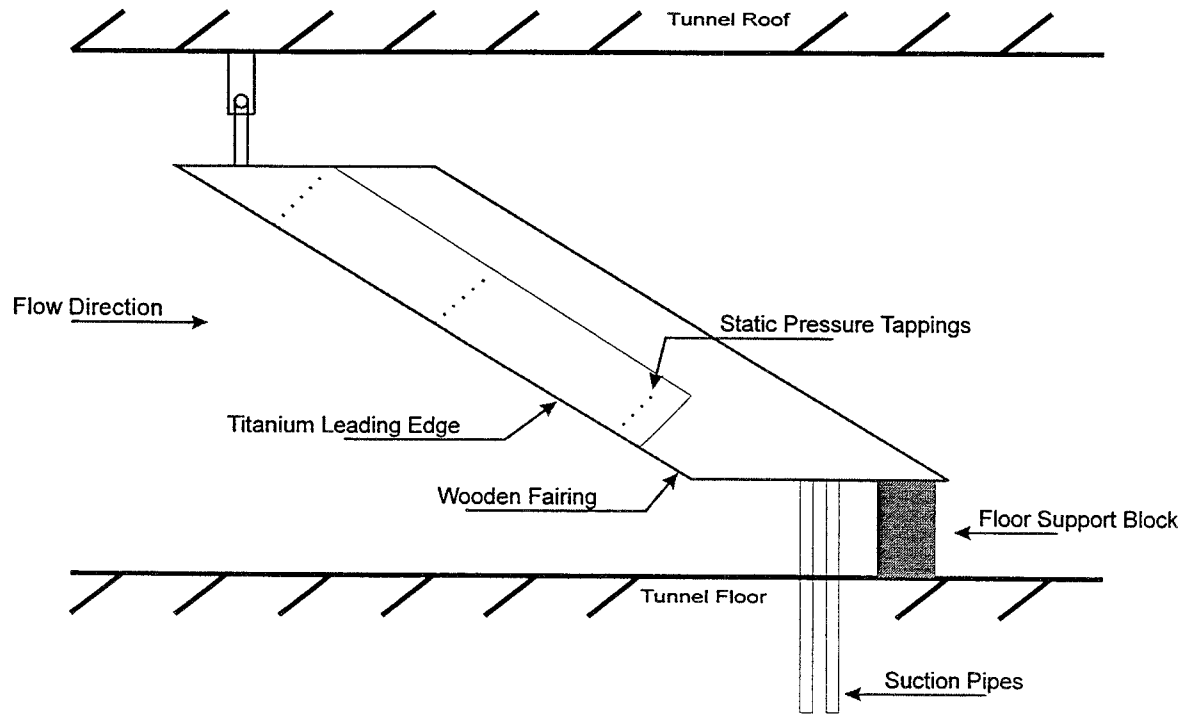

Figure 5. Arrangement of The Model in The CoA 8'x6' Wind Tunnel

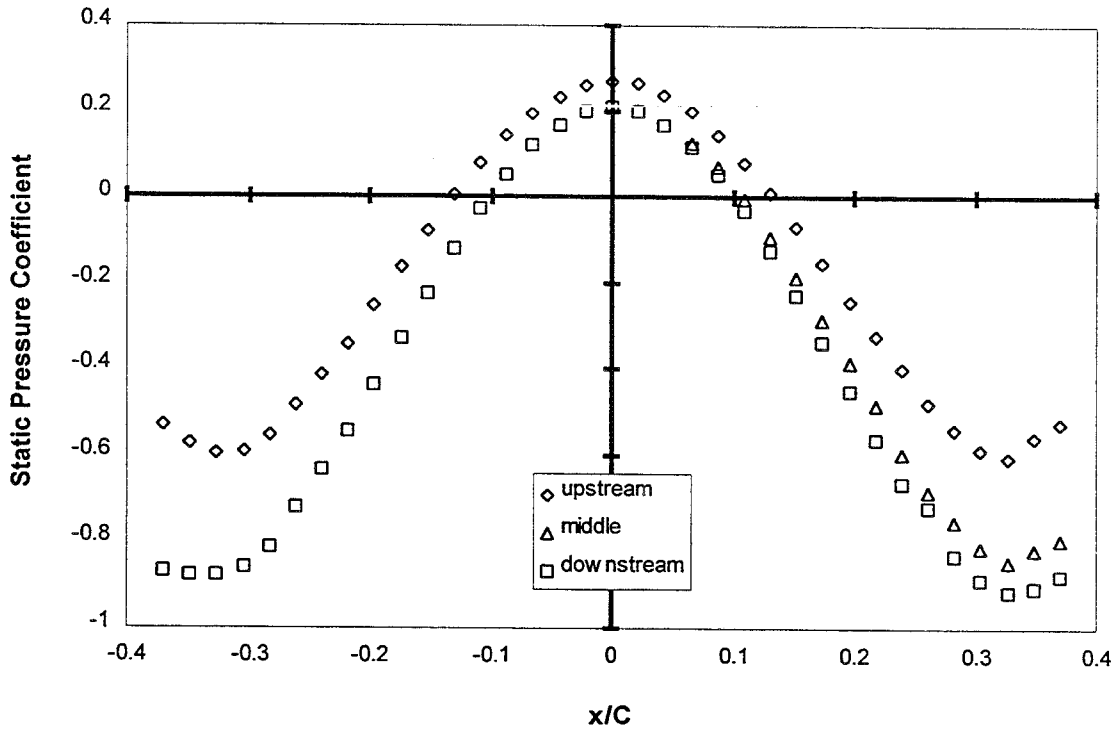

Figure 6. Sample Static Pressure Coefficient Distribution Around Leading Edge

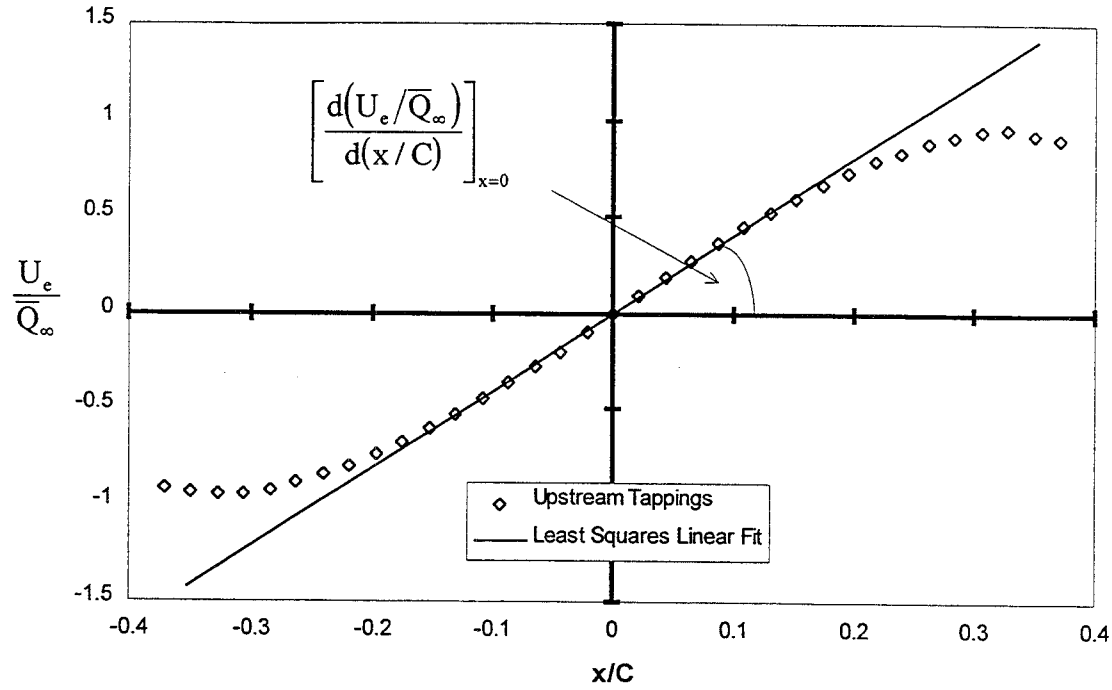

Figure 7. Typical Non-Dimensional Chordwise Velocity distribution

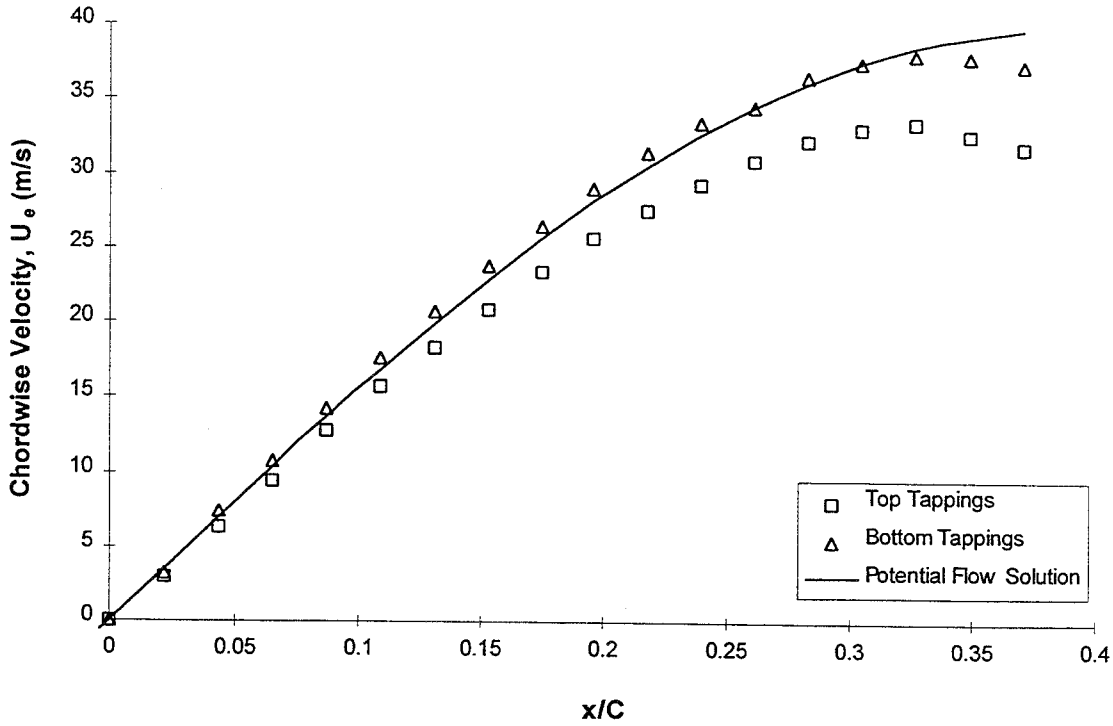

Figure 8. Chordwise Velocity Distribution Compared With The Potential Flow Solution

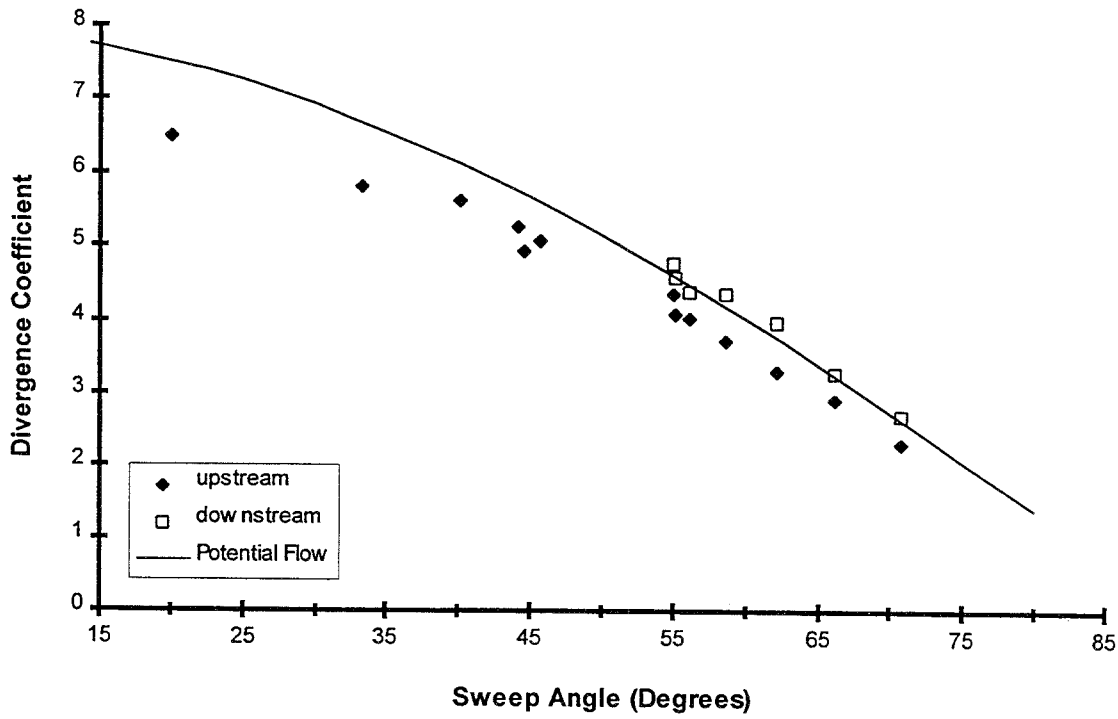

Figure 9. Comparison of Experimental Divergence Coefficients With Potential Flow Solution

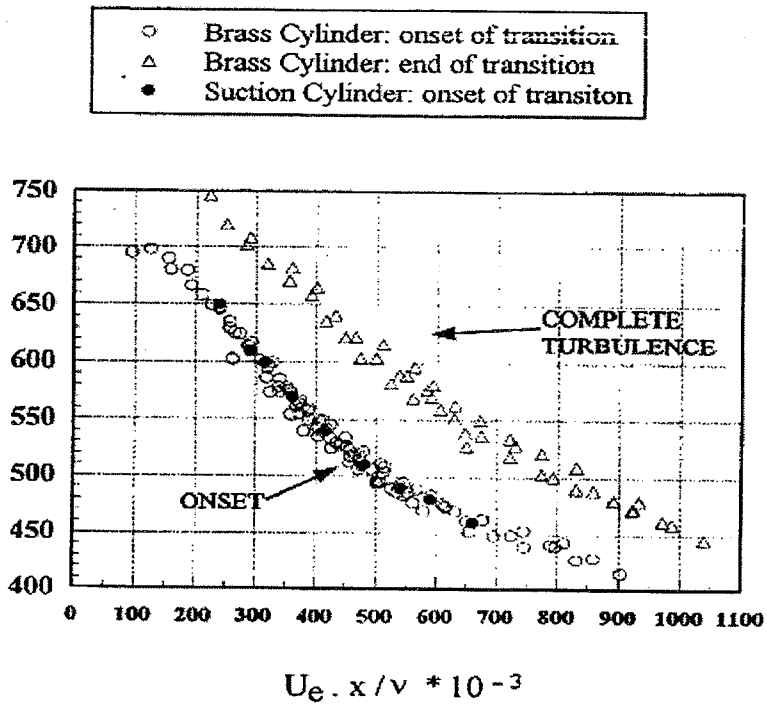

Figure 10. Conditions for the Onset and End of Transition Caused by Cross-Flow Instability, after Danks

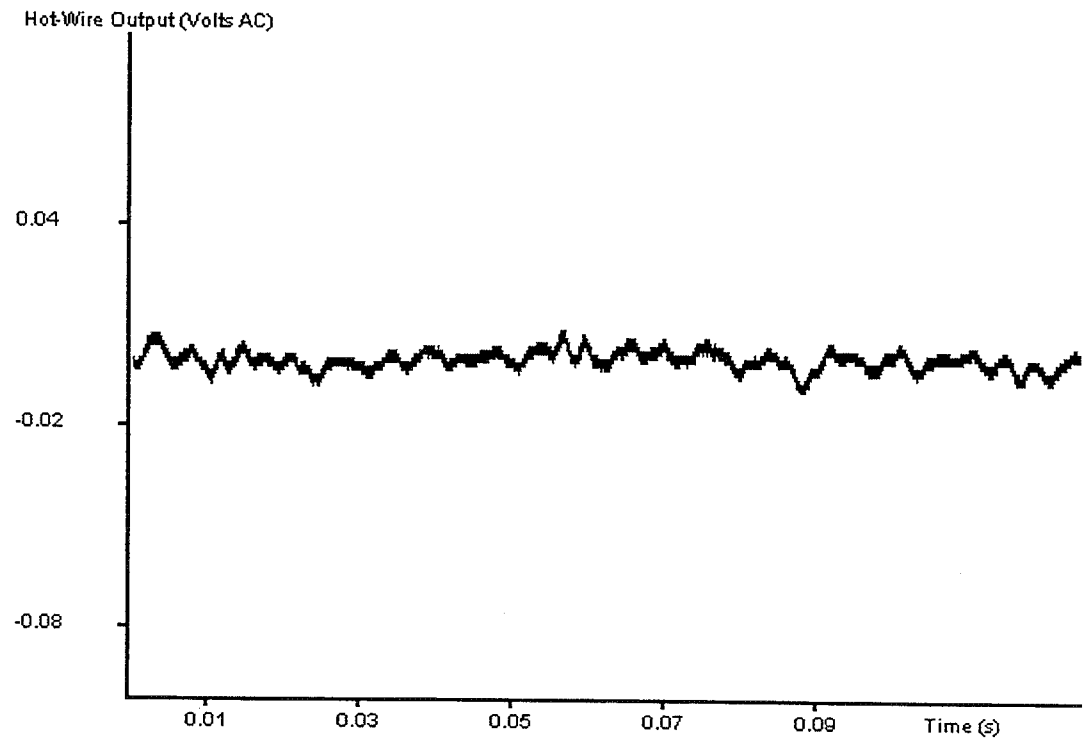

Figure 11. Typical Output from Hot Wire For A Stable Laminar Boundary Layer

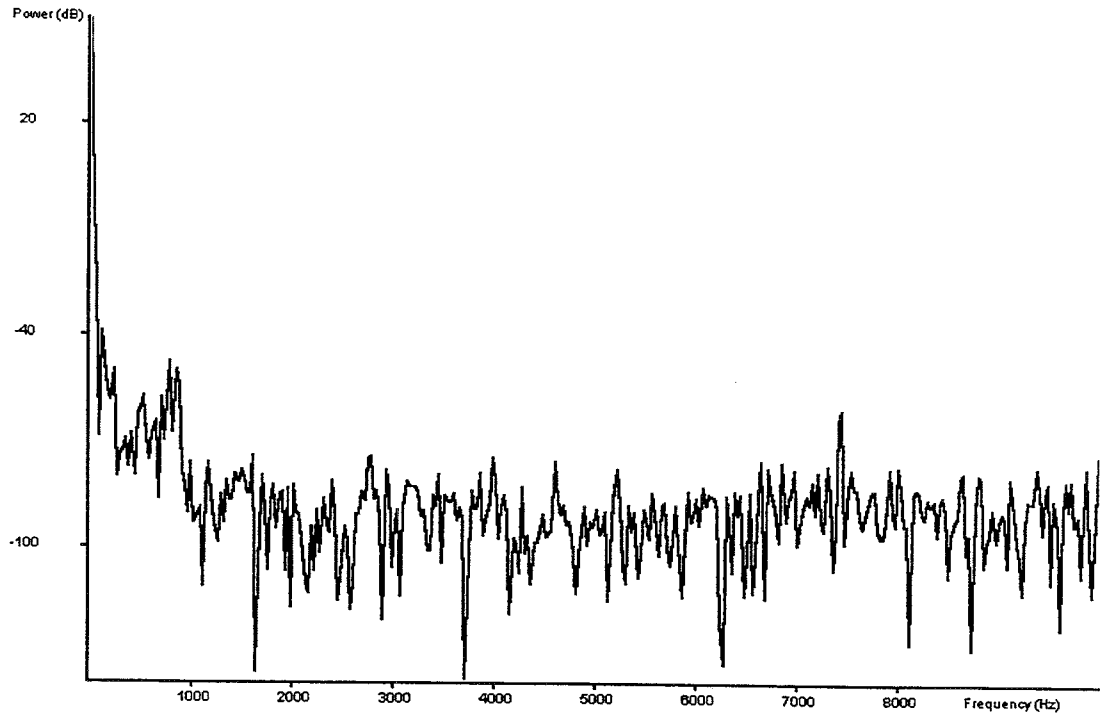

Figure 12. Power Spectrum Of A Stable Laminar Boundary Layer

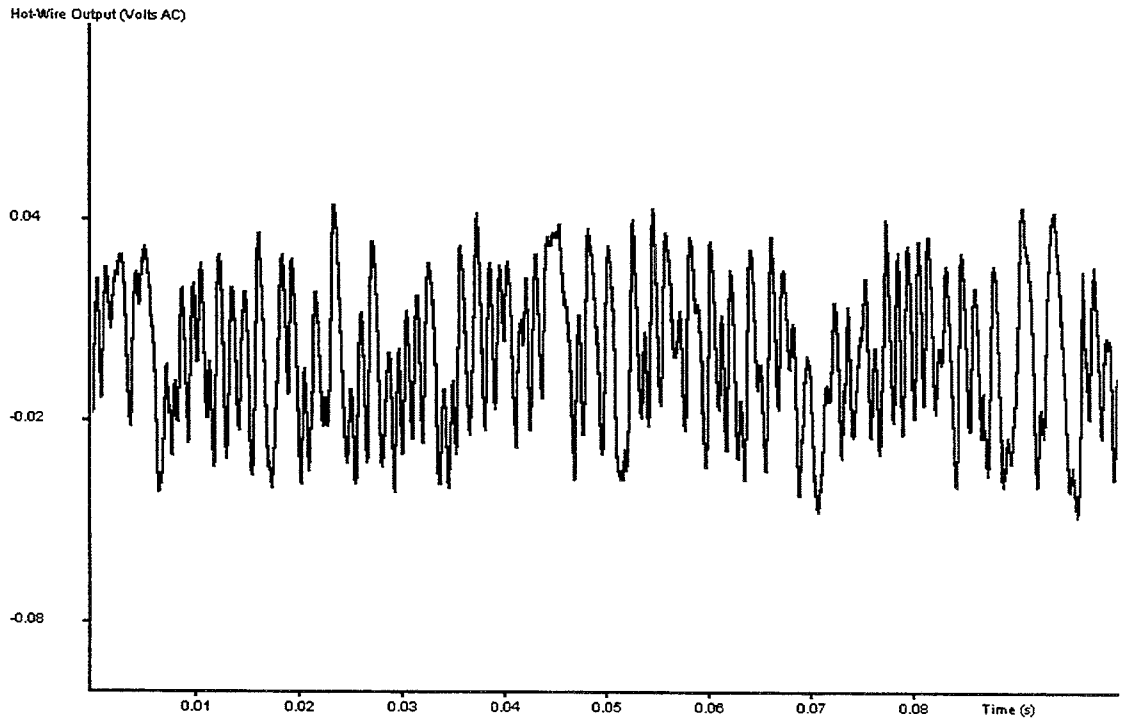

Figure 13. Typical Output from Hot Wire For Laminar Boundary Layer With Unstable Laminar Disturbances

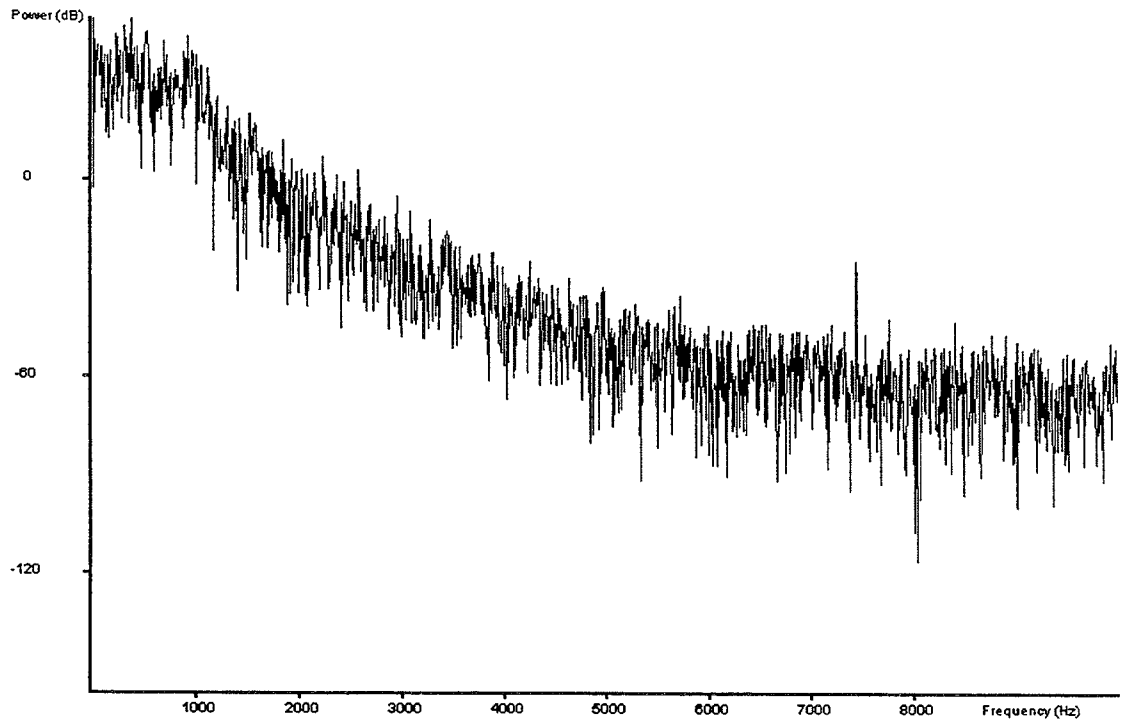

Figure 14. Power Spectrum of Laminar Boundary Layer With Unstable Laminar Disturbances

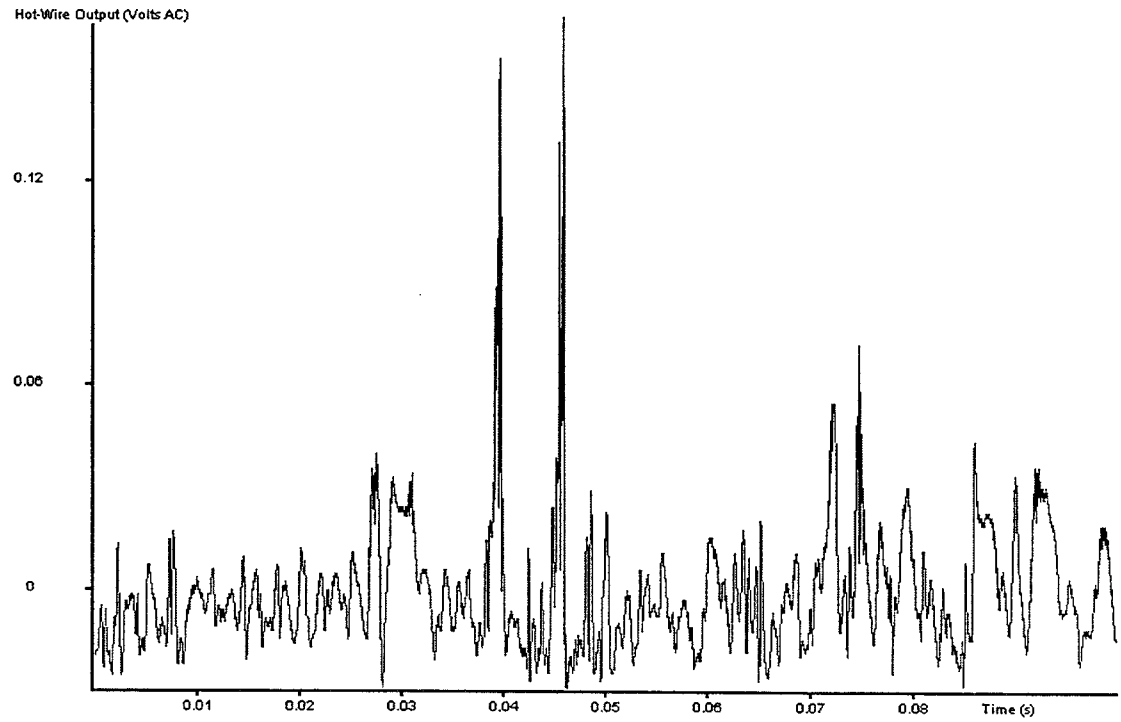

Figure 15. Typical Output from Hot Wire For The Onset of Transition: Laminar Boundary Layer With Unstable Laminar Disturbances And Turbulent Bursts

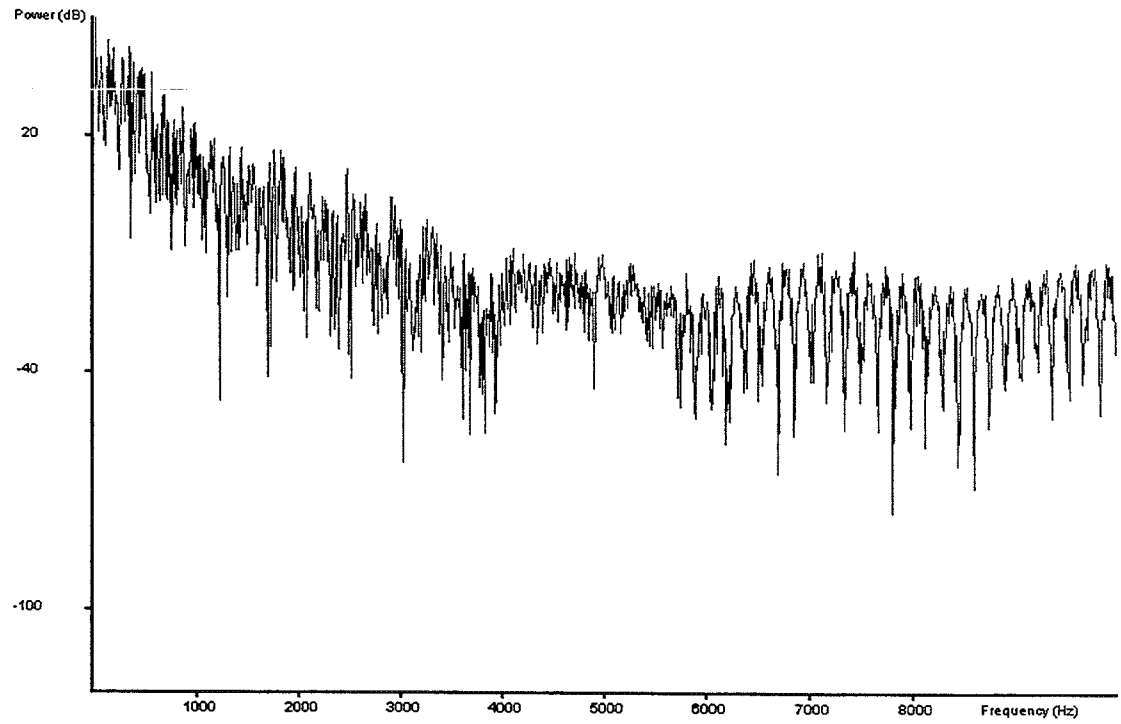

Figure 16. Power Spectrum of Laminar Boundary Layer With Unstable Laminar Disturbances and Turbulent Bursts

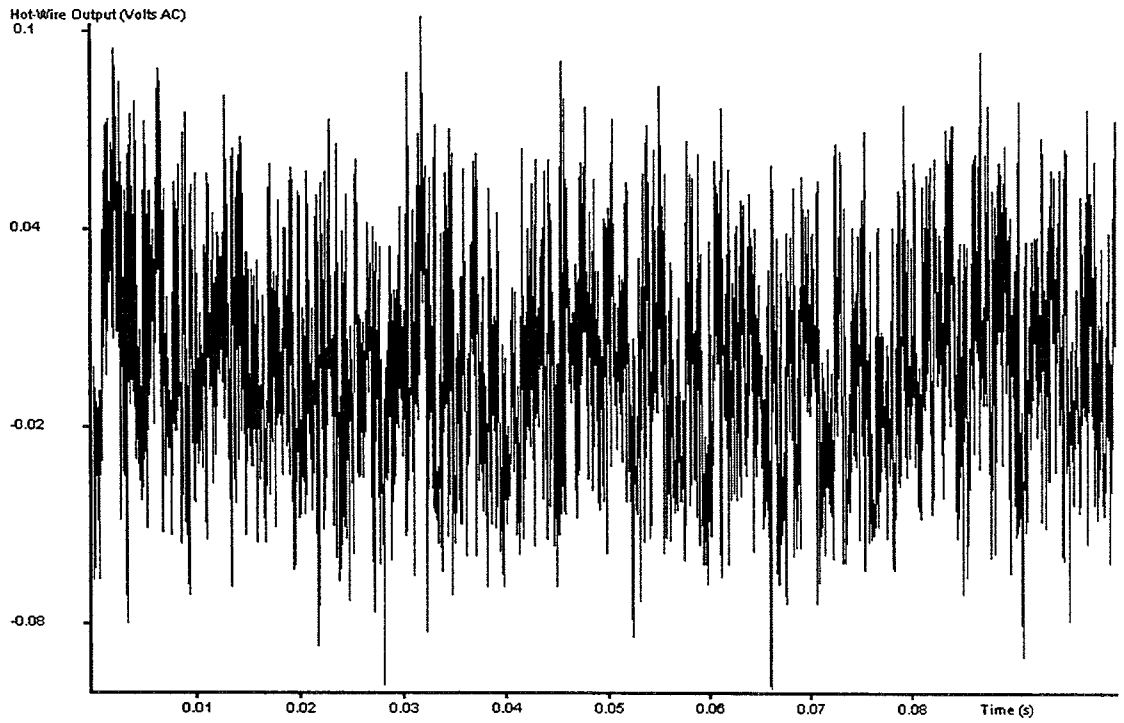

Figure 17. Typical Output From Hot Wire For Turbulent Boundary Layer

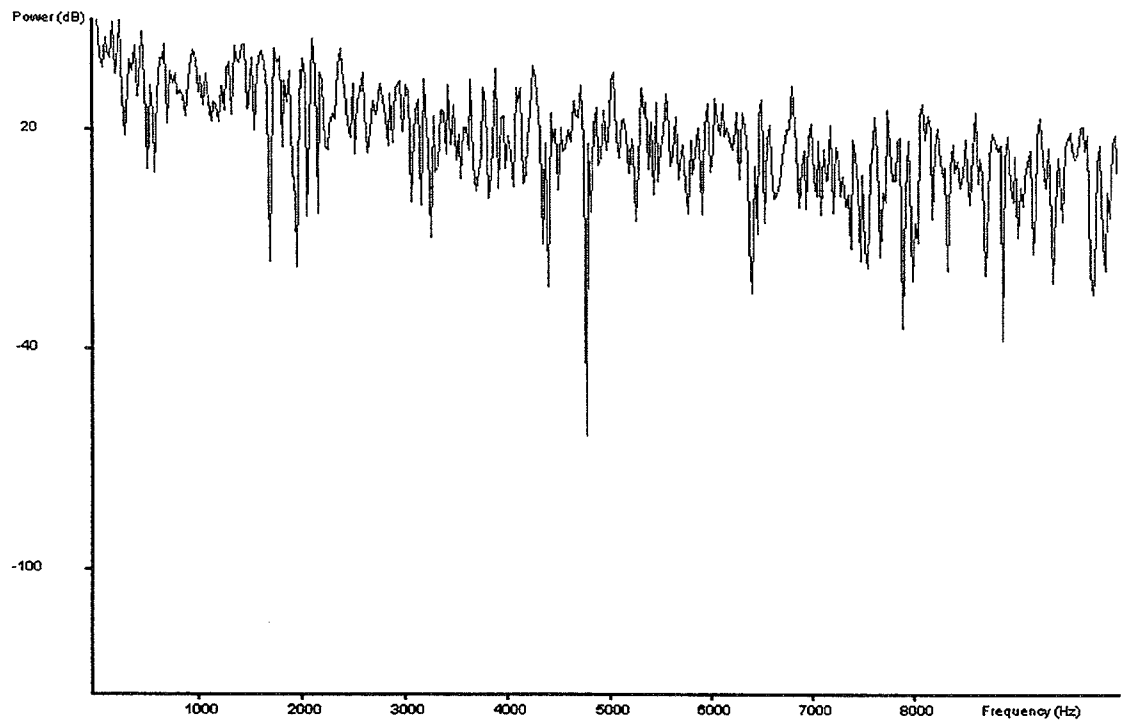

Figure 18. Power Spectrum of Turbulent Boundary Layer

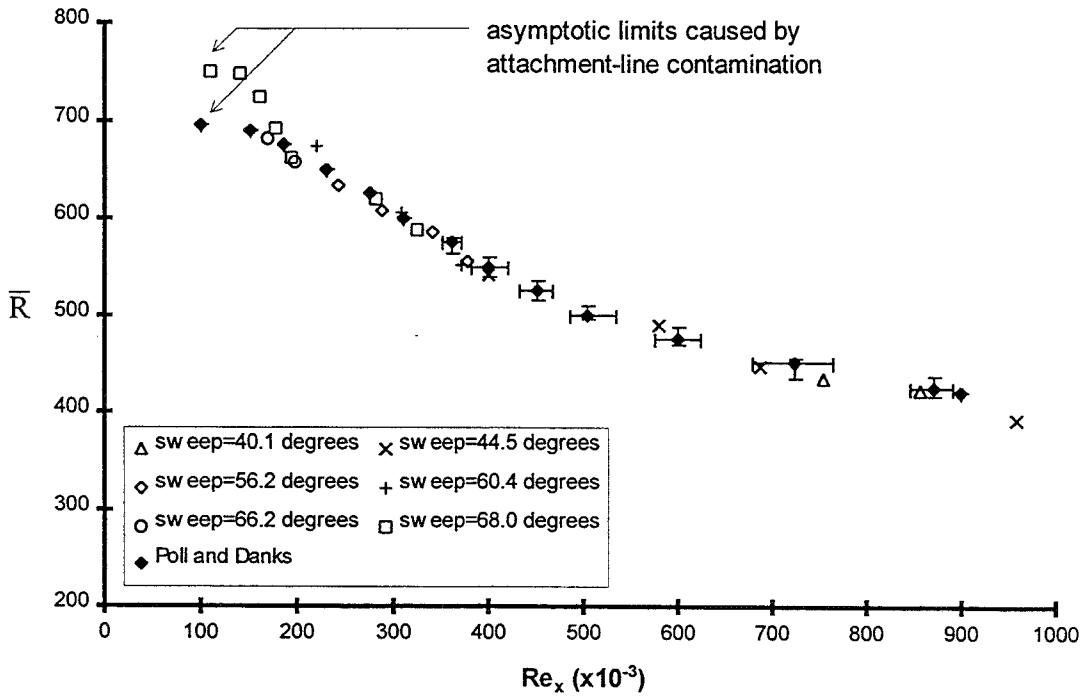

Figure 19. Natural Transition on a Non-Porous Surface and Comparison With Previous Work

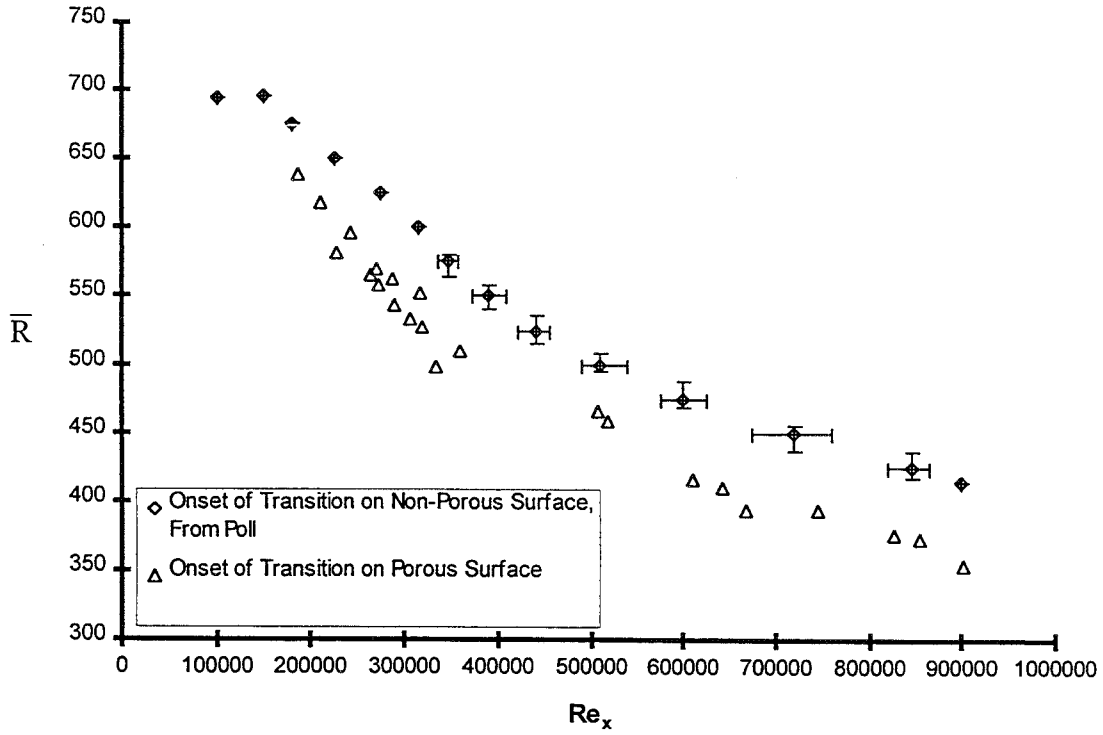

Figure 20. Comparison of the Onset of Transition on Porous and Non-Porous Surfaces

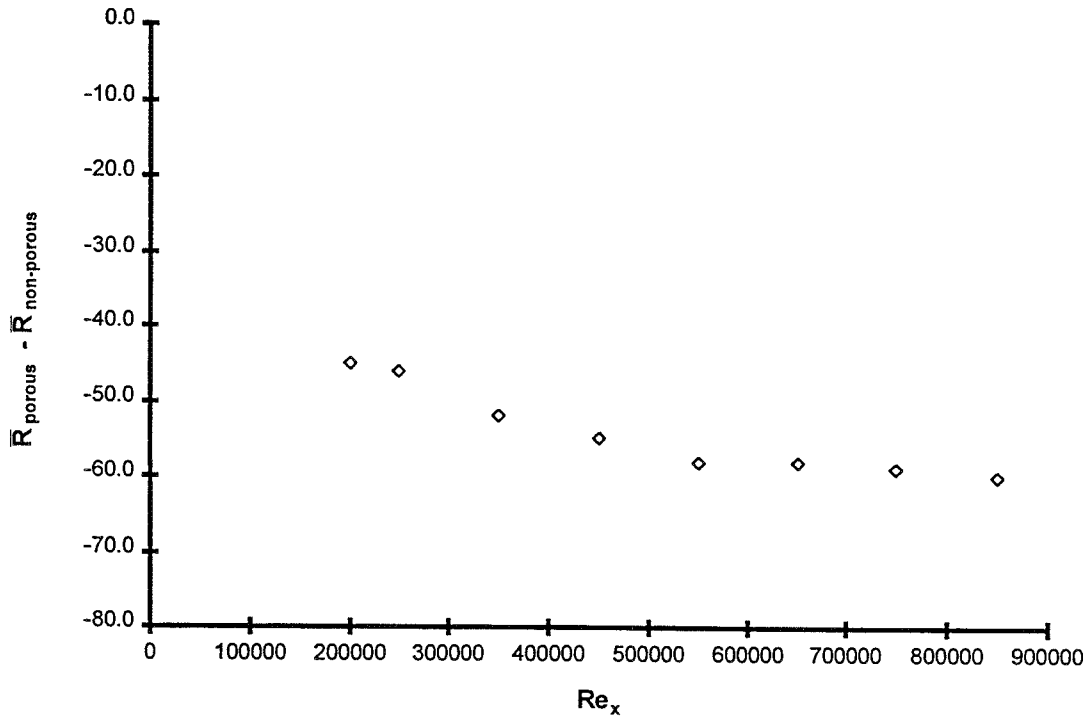

Figure 21. The Reduction of $\bar{R}$ Due To The Porous Surface

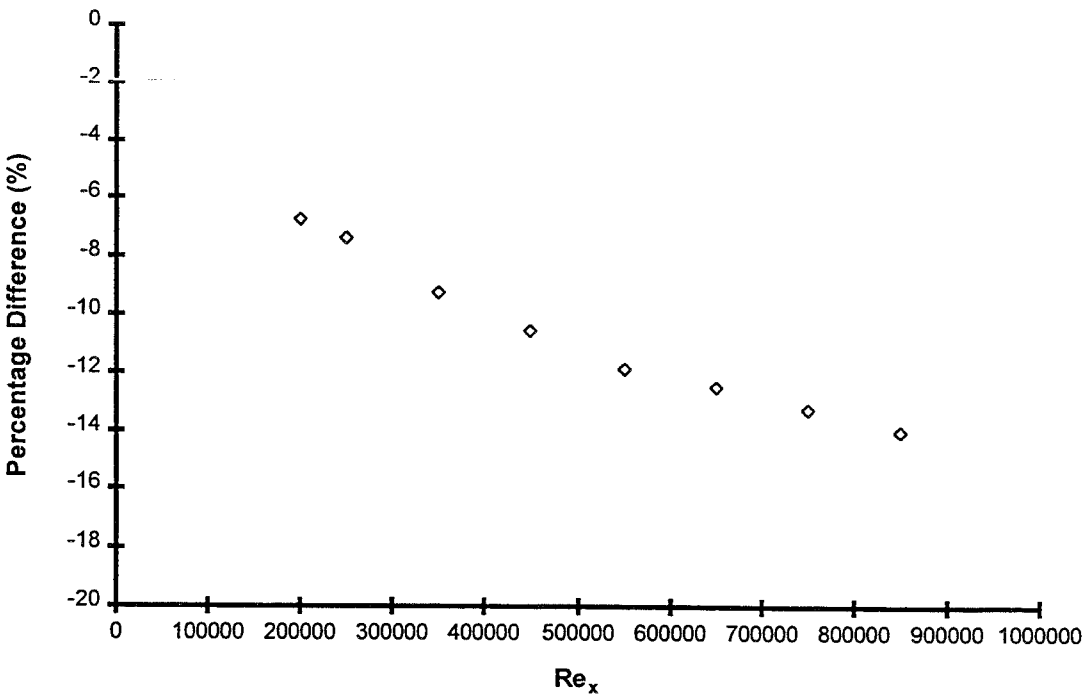

Figure 22. Percentage Reduction of $\bar{R}$ Due To The Porous Surface

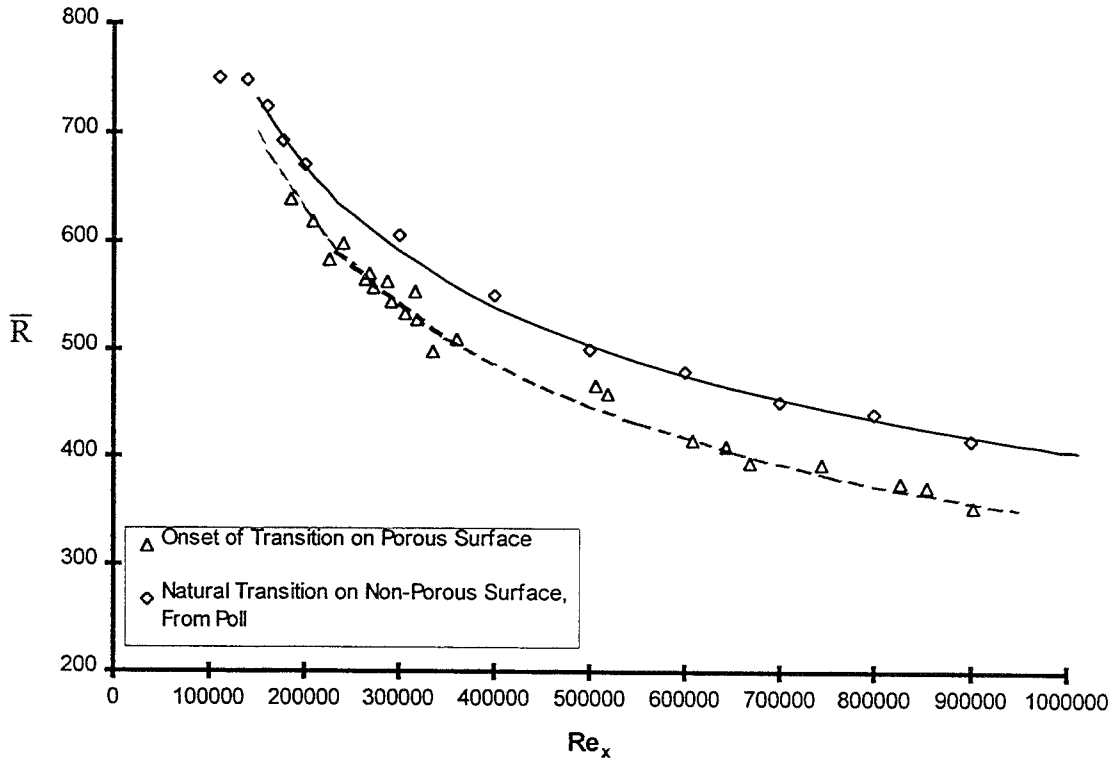

Figure 23. Comparison of Power Law Approximations With Experimental Data

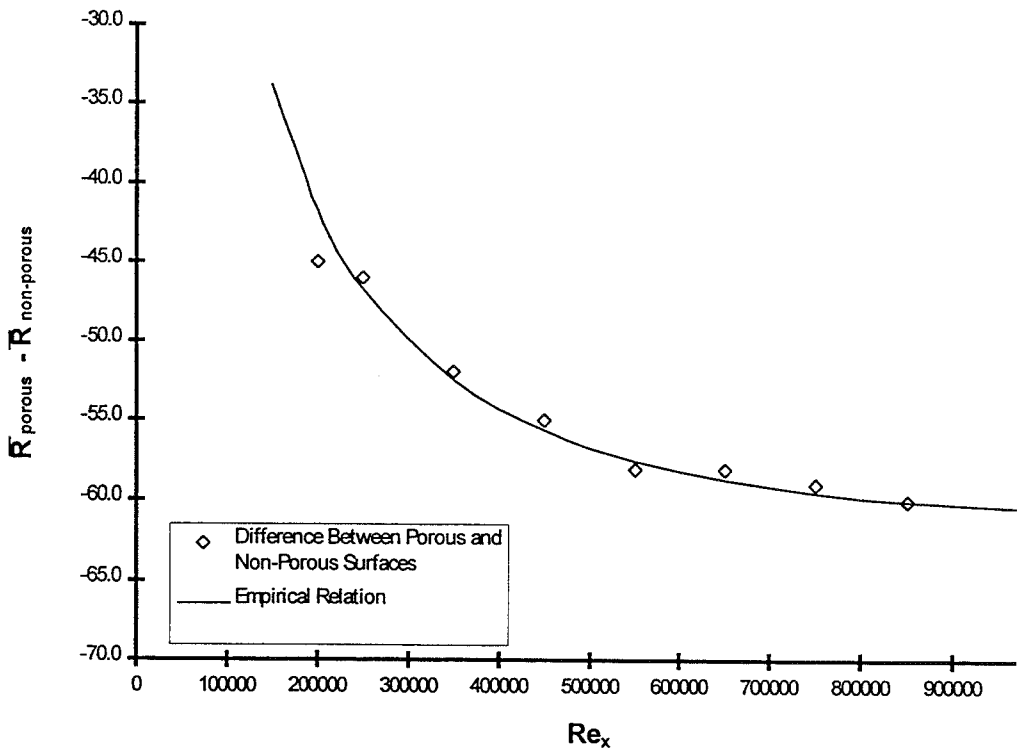

Figure 24. Comparison of Measured $\overline{R}$ Reduction With Empirical Relation

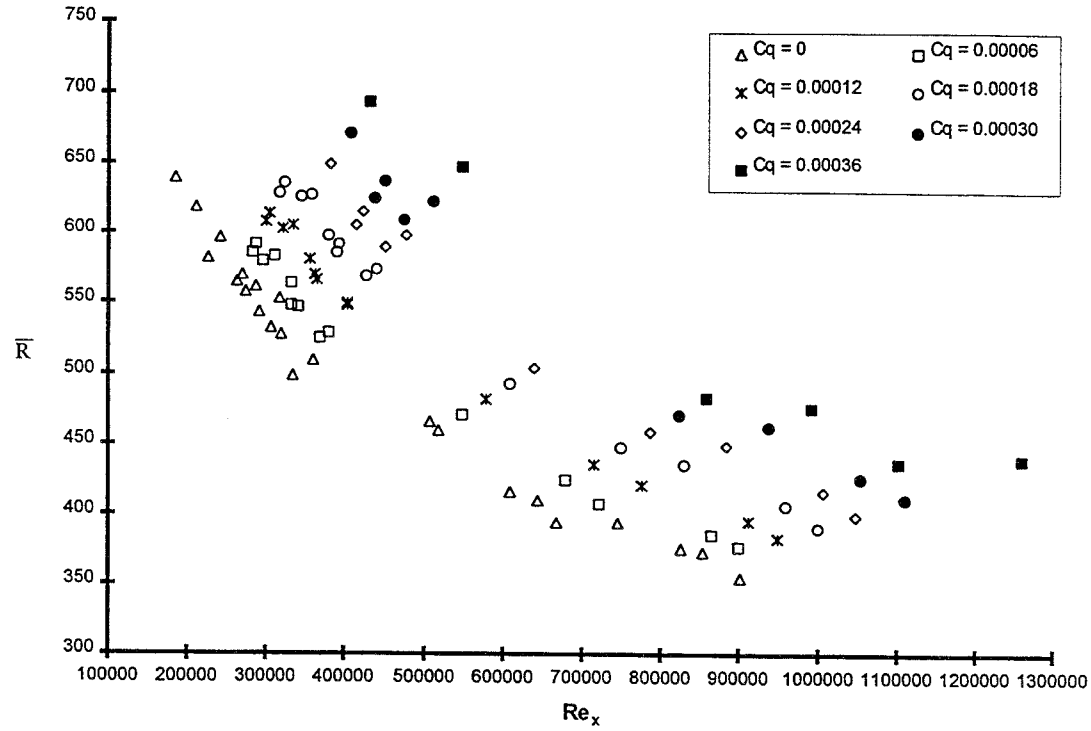

Figure 25. The Effect of Uniform, Distributed Suction On The Onset Of Transition Through Cross-Flow Instability

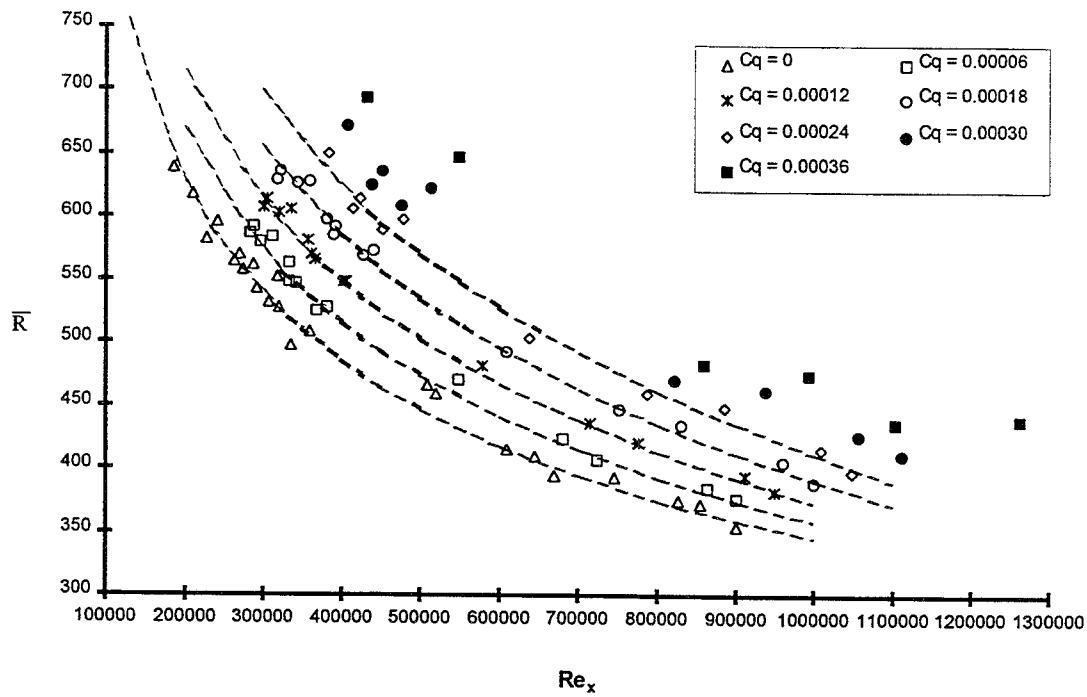

Figure 26. Comparison of Power Law Curve Fits With Experimental Data

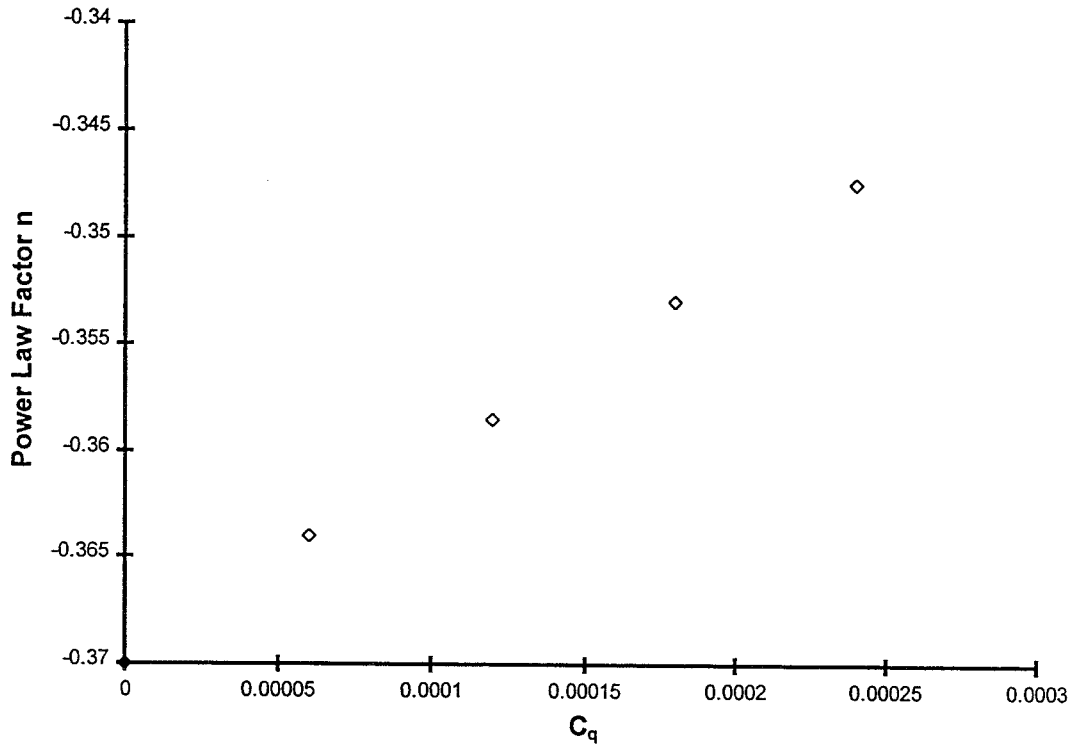

Figure 27. Variation of Empirical Relation Coefficient n With C_q

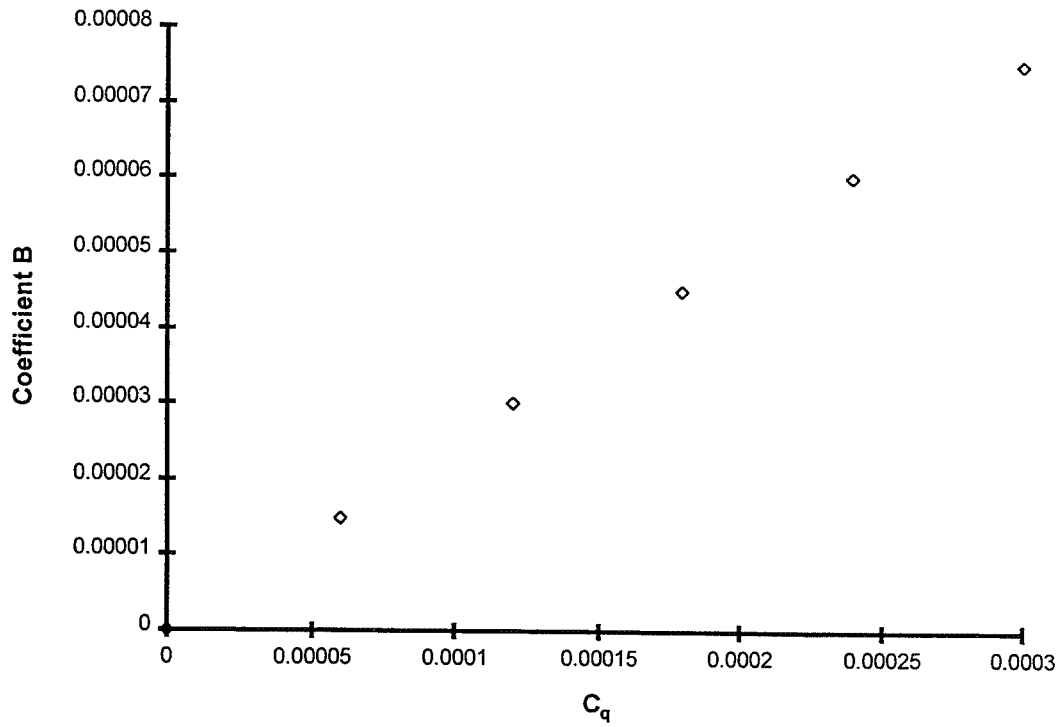

Figure 28. Variation of Empirical Relation Coefficient B With C_q

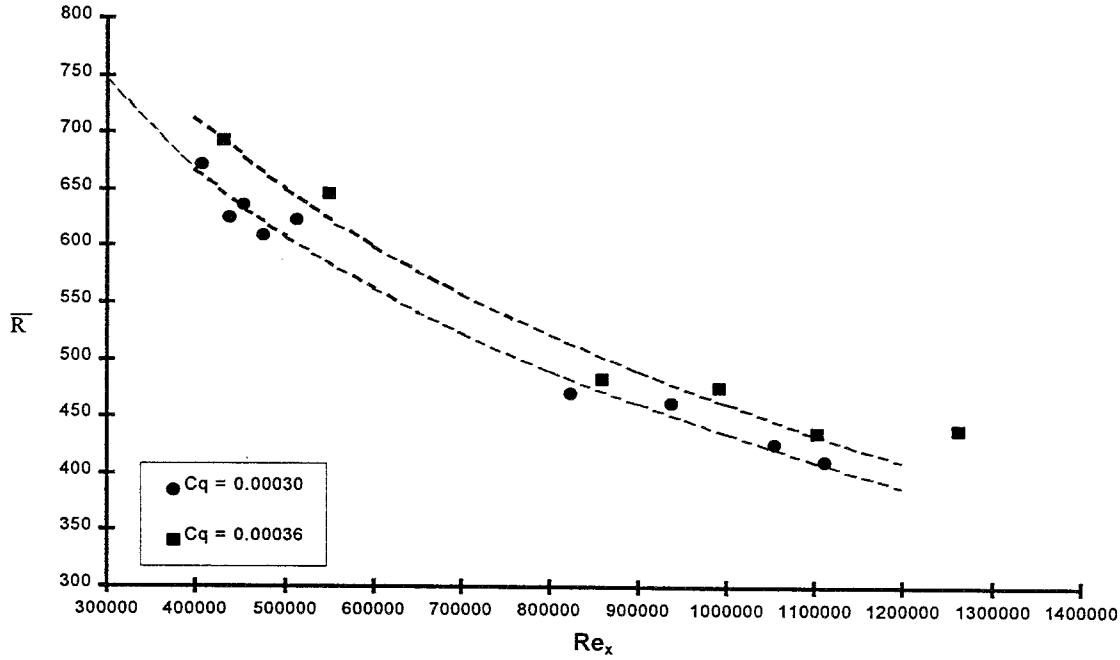

Figure 29. Curve Fits Calculated From Empirical Relation

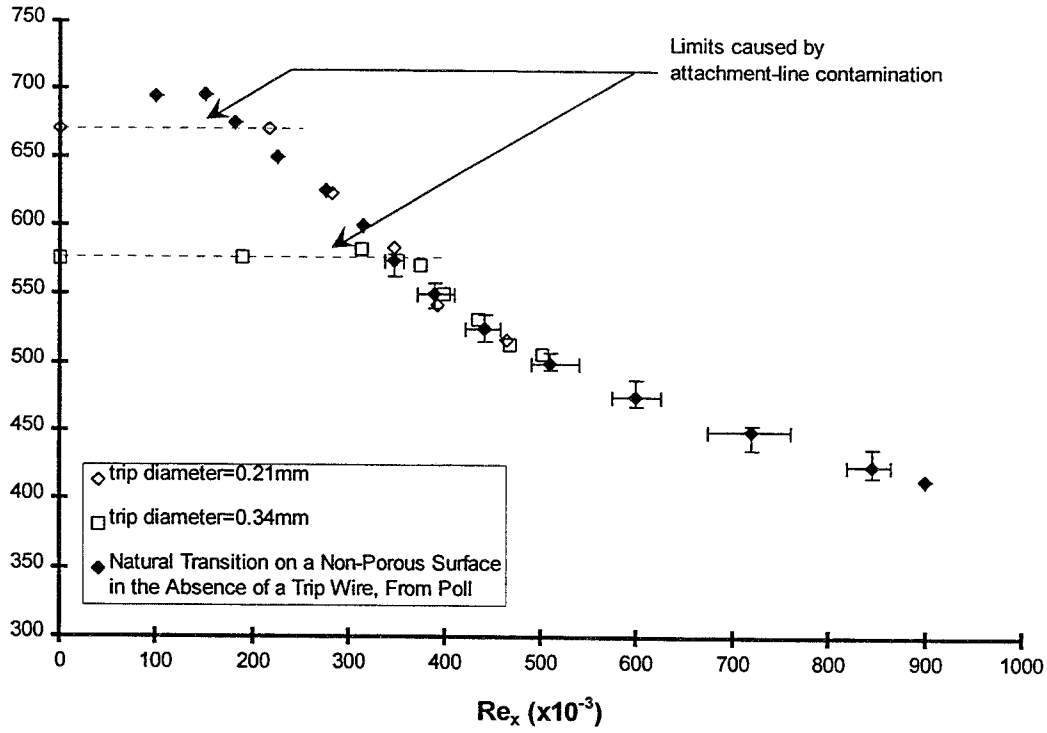

Figure 30. Transition Characteristics With a Two-Dimensional, Trip Wire On A Non-Porous Surface

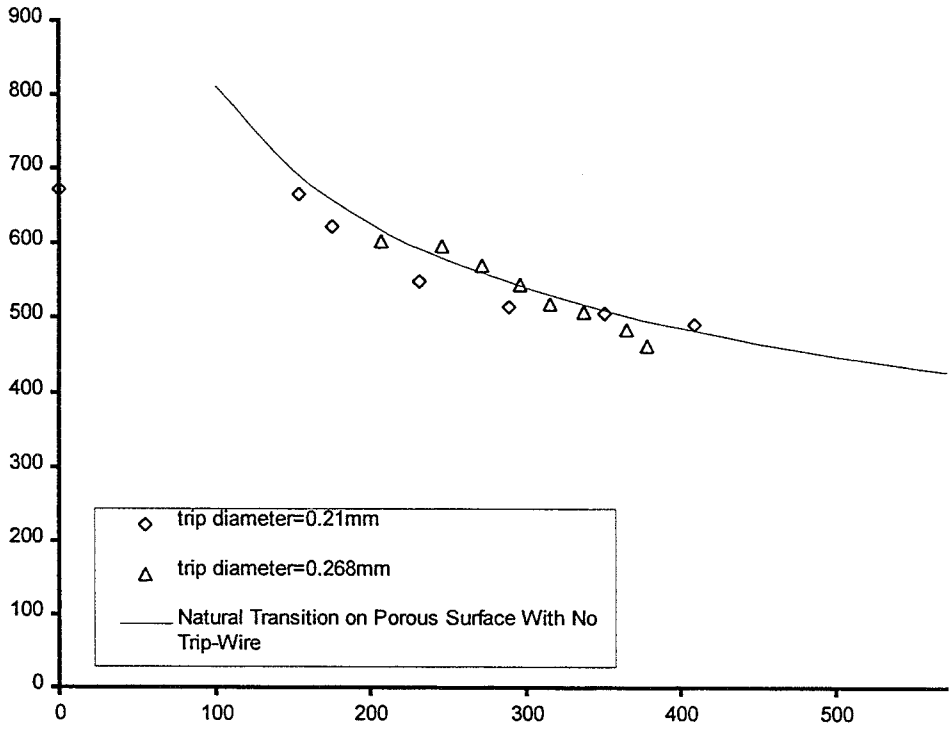

Figure 31. Transition Characteristics on a Porous Surface With a Two-Dimensional Trip Wire